Copyright Warning & Restrictions

The copyright law of the United States (Title 17, United States Code) governs the making of photocopies or other reproductions of copyrighted material.

Under certain conditions specified in the law, libraries and archives are authorized to furnish a photocopy or other reproduction. One of these specified conditions is that the photocopy or reproduction is not to be "used for any purpose other than private study, scholarship, or research." If a, user makes a request for, or later uses, a photocopy or reproduction for purposes in excess of "fair use" that user may be liable for copyright infringement,

This institution reserves the right to refuse to accept a copying order if, in its judgment, fulfillment of the order would involve violation of copyright law.

Please Note: The author retains the copyright while the New Jersey Institute of Technology reserves the right to distribute this thesis or dissertation

Printing note: If you do not wish to print this page, then select "Pages from: first page # to: last page #" on the print dialog screen

NJIT
New Jersey's Science & Technology University

The Van Houten library has removed some of the personal information and all signatures from the approval page and biographical sketches of theses and dissertations in order to protect the identity of NJIT graduates and faculty.

ABSTRACT

Processing, Structural and Electrical Properties of SiC

by
Mark Farhad-Garousi

Cubic silicon carbide films grown by chemical vapor deposition (CVD) on silicon substrates typically have n-type conductivity at 300 °K dominated by a heavily compensated donor with a binding energy in the < 20 meV range. Binding energies <20 meV are not expected in SiC for isolated donors because the shallowest expected binding energy for an electron bound to an isolated donor is approximately 47 meV. The work done on this topic by a few group of scientists has been studied.

PROCESSING, STRUCTURAL AND ELECTRICAL PROPERTIES OF SiC

by
Mark Farhad-Garousi

A Thesis
Submitted to the Faculty of
New Jersey Institute of Technology
in Partial Fulfillment of the Requirements for the Degree of
Master of Science in Engineering Science

Committee for the Interdisciplinary Program
in Materials Science and Engineering Program

May 1994

APPROVAL PAGE

PROCESSING, STRUCTURAL AND ELECTRICAL PROPERTIES OF SiC

Mark Farhad-Garousi

Dr. N. M. Ravindra, Thesis Advisor Date
Associate Professor
Physics Department, NJIT

Dr. Onforio Russo, Committee Member Date
Associate Professor
Physics Department, NJIT

Dr. Leon Buteau, Committee Member Date
Acting Chairman
Physics Department, NJIT

BIOGRAPHICAL SKETCH

Author: Mark Farhad-Garousi

Degree: Master of Science in Engineering Science

Date: May 1994

Undergraduate and Graduate Education:

- Master of Science in Engineering Science
  New Jerssey Institute of Technology,
  Newark, New Jersey, 1994

- Bachelor of Arts in Physics
  Rutgers University
  Camden, New Jersey, 1988

Major: Physics of Electronic Materials

This thesis is dedicated to
New Jesey Institute of Technology

ACKNOWLEDGMENT

The author wishes to express his sincere gratitude to his thesis advisor, Dr. N.M. Ravindra for his guidance, friendship and advice throughout this research.

Special thanks to Dr. Leon Buteau, Acting Chairman of Physics Department and Dr. Onofrio Russo for serving as members of the committee.

The author is grateful to The Department of Physics at NJIT and The State of New Jersey Department of Labor for their financial support.

The author is deeply indebted to his parents and family for their endless love, support, encouragement and patience.

TABLE OF CONTENTS

Chapter | Page

1 INTRODUCTION.. 1

2 CRYSTAL STRUCTURE................................... 4

2.1 Introduction.......................................4

2.2 Polymorphism and Polytypism........................4

2.3 SiC Bonding..5

2.4 SiC Network..5

2.5 Ramsdel Notation...................................8

2.6 Some Explanations for Polytype Formation...........8

3 PREPARATION METHODS.................................12

3.1 Historical Overview of SiC Research...............12

3.2 Growth Methods 13

3.2.1 Conventional Methods............................13

3.2.1.1 Acheson Method................................13

3.2.1.2 The Method of Gaseous Cracking................15

3.2.1.3 The Method Of Sublimation (Lely Method)........................15

3.2.1.4 The Method Of Crystallization from Solution.......................................16

3.2.2 Recent Methods..................................17

3.2.2.1 The Modified Sublimation Process..............17

3.2.2.2 Heteroepitaxial Growth of SiC by CVD..........................19

3.2.2.2 Plasma Enhanced CVD...........................21

TABLE OF CONTENTS
(continued)

Chapter **Page**

4 PROPERTIES....24

4.1 Electrical Properties....24

4.1.1 Review of Prior Hall and related studies on SiC....24

4.1.2 Temperature Dependence of Electical Properties of ß-SiC Grown By CVD....28

4.1.2.1 K. Sasaki et al. (1984)....29

4.1.2.2 B. Segal et al. (1986)....32

4.1.2.3 M. Yamanaka et al. (1987)....35

4.1.2.4 A. Suzuki et al. (1988)....42

4.1.2.5 T.Tachibana et al. (1990)....44

5 CONCLUSIONS....48

APPENDICES

1 Comparison of Properties of Semiconductors....50

2 The More Common SiC Polytypes....51

3 SiC Phase Diagram....52

4 Theoretical Calculation of Hall Mobility and Compensation Model....55

LIST OF FIGURES

Figure		Page
2.1	Zincblende structure with cubic and hexagonal unit cell	6
2.2	Structural unit slabs of (a) close packed element structure types; (b) Binary tetrahedral structure types	7
3.1	Growth cavity used in the sublimation (Lely) process	16
3.2	Crucible assembly for the growth of SiC single crystals by the modified Lely method	18
3.3	Process steps for growing ß-SiC on Si	20
3.4	Phase diagram of SiC	52
3.5	Growth rate vs temperature (a,b)	53
3.6	(a,b) Growth rate vs flow rate.	54
4.1	(a) Hall mobilities μ_H of three samples of 3C-SiC epilayers as a function of temperature. (b) Temperature dependence of conductivity σ, carrier concentration n, and Hall mobility μ_H of a 3C-SiC epilayer	30
4.2	Carrier concentration n vs. 1000/T. The points are experimental results [28] while the continuous and dashed lines are calculated fits using compensation and noncompensation, respectively. (a) Three cubic SiC samples. (b) A self-supporting sample	33
4.3	Donor activation energy E_D vs donor density N_D. The continuous line is given by Eq. (4.2) using E_D (0)=48 meV and α=2.6X10^{-5} meV cm	35
4.4	Temperature dependence of (a) carrier density and (b) Hall mobility of an unintentionally doped n-type 3C-SiC epilayer with calculated values denoted by a solid curve. Dashed and dot-dashed curves denote temperature dependencies of electron mobilities of 15R-SiC and 6H-SiC, respectively	37
4.5	Al/Si ratio dependencies of carrier concentration and Hall mobility of Al-doped 3C-SiC	38

LIST OF FIGURES
(continued)

Figure | Page

4.6 Temperature dependencies of (a) carrier densities (b) Hall mobilities of two Al-doped p-type 3C-SiC epilayers with calculated values denoted by solid and dashed curves....................................41

4.7 Temperature dependencies of Hall mobility of (a) undoped. (b) Nitrogen-doped films. Solid, and dotted lines are calculated values...............60

4.8 Temperature dependence of (a) resistivity, (b) carrier concentration (solid lines represent theoretical data), and (a) electron Hall mobility of ß-SiC chemically vapor deposited on Si (100). Numbers shown in the legend refer to experimental sample numbers. See table 4.5 for data regarding the properties of these films........................45

4.9 Temperature dependence of (a) resistivity, (b) carrier concentration (solid line represents theoretical data), and (c) electron Hall mobility of ß-SiC chemically vapor deposited on off-axis Si (100). Numbers shown in the legend refer to experimental sample numbers. See table 4.6 for data regarding the character of these films...............63

4.10 Temperature dependence of (a) resistivity, (b) carrier concentration (solid line represents theoretical data), and (c) electron Hall mobility of an undoped ß-SiC (111) film grown directly on an α(6H)-SiC (0001) Lely crystal. In (a) the estimated values (substrate) and the calculated values for the grown film (film) are also plotted. In (b) the values for the grown film calculated (film) using the estimated values of resistivity are also plotted. See table 4.7 for data regarding the nature of this sample............................64

4.11 Temperature dependence of (a) resistivity, (b) carrier concentration (solid line represents theoretical data), and (c) electron Hall mobility of an undoped α-SiC film grown directly on an off -axis α(6H)-SiC Lely crystal. In (a) the estimated values (substrate) and the calculated values for the grown film (film) are also plotted. In (b) the values for the grown film calculated (film) using the estimated values of resistivity are also plotted. See table 4.7 for data 65

LIST OF TABLES

Table page

1.1 Comparison of semiconductors........................50

2.1 Some of the known SiC polytypes......................9

2.2 Selected SiC polytypes..............................51

4.1 Parameters and errors estimates obtained in a liearized least-squares fit using a compensated model.................................34

4.2 Donor ionization energies E_D donor N_D, Acceptor concentrations N_A, and compensation ratio N_A/N_D obtained from a least-squares fit of the data Suzuki et al. to the single-level expression for the carrier concentration using the band parameters discussed in the source of this table....44

4.3 Numerical values used for theoretical calculations..59

4.4 Donor concentration N_D, acceptor concentration N_A, and compensation ratio N_A/N_D obtained from theoretical calculations fitted to the experimental data of Hall mobility...............................60

4.5 Parameters obtained by fitting the compensation model to carrier-concentration vs temperature data obtained for ß-SiC (100) on Si (100)...........47

4.6 Parameters obtained by fitting the compensation model of carrier-concentration vs temperature data obtained for ß-SiC (100) on off-axis Si (100)...63

4.7 Parameters obtained by fitting the compensation model to the values of carrier-concentration vs temperature calculated by assuming the resistivity of the substrate for carrier concentration vs temperature for unintentionally doped ß-SiC and α-SiC grown directly on Lely crystals...........64

CHAPTER 1

INTRODUCTION

Significant progress has been made recently in the crystal growth and semiconductor device technology of SiC. Advances in the growth of both ß (3C)- SiC and α (6H)- SiC have been made. Advances in device technology include the development of a 650 °C metal-oxide-semiconductor field-effect transistor (MOSFET), and improved processes for ion implantation and plasma-assisted etching[1]. The trend towards more electronic devices and sensors in propulsion and power systems is inexorable. The need for higher performance and efficiency requires more control over the many elements of these systems. Hence, there is a growing need for sensors with integrated electronics, power electronics for actuators and distributed microcomputer chips.

In many applications, the temperature and sometimes radiation is approaching or exceeding the limits of commercially available semiconductors. As the temperature rises, the reliability of devices goes down. An example is the automobile engine which is bing designed to run hotter and at the same time use more electroninc devices for control and diagnostics. This has forced the placement of some electronics in cooler locations away from the engine which in turn makes the electronics suceptable to electrical

noise. In advanced turbine engines, there is a need for control and monitoring electronics that are not constrained to temperature-controlled environments. The goal is increased flexibility in the use of electronics, with the benefit being increased performance and elimination of cooling. In space power systems, there is a need for high temperature power conversion electronics. In this application, higher operating temperatures leads to much smaller radiators that are used to get rid of waste heat due to power conversion losses.

Component reliability is a key issue in all aerospace applications. Because of its ceramic character, it is believed that the potential reliability of semiconductor devices and sensors fabricated from SiC will be much higher than that obtained from any other semiconductor material. This reliability advantage should hold for all operating temperatures.

Other potentially important applications of SiC are in light-emitting diodes (LED) (using 6H SiC) and in high frequency components. The high frequency applications could ultimately have the greatest commercial impact of all SiC applications considered so far.

The entire content of this work is solely a literature survey from the theoretical and experimental results published by a few groups of scientists. The crystal structure and the growth methods are described in chapters

2 and 3 respectively. The major emphasis is on the electrical properties of ß-SiC in chapter4.

CHAPTER 2

CRYSTAL STRUCTURE

2.1 Introduction

SiC is known to crystallize into over 170 orderly modifications; and its crystal structure is characterized by a special case of one dimensional polymorphism known as polytypism.

2.2 Polymorphism and Polytypism

The concept of polymorphism which is restricted solely to crystalline modifications[2] has been described as the phenomenon of the same chemical substance crystallizing in more than one structure. The different structures are called polymorphs or polymorphic modifications.

Polytypism and polytypic structures have been defined as the ability of a substance to crystallize into a number of different modifications, in all of which two dimensions of the unit cell are the same while the third is a variable integral multiple of a common unit. The different polytypic modifications can be regarded as build up of layers of structures stacked parallel to each other at constant intervals along the variable dimension. The two unit-cell dimensions parallel to these layers are the same for all the modifications. The third dimension depends on the stacking sequence, but is always an integral multiple of the layer

spacing. Different manners of stacking these layers may result in structures having not only different morphologies but even different lattice types and space groups.

2.3 SiC Bonding

According to valance bond theory [3], each group IVA atom must make available for bonding four equivalent orbitals and four unpaired electrons. To do this, each carbon and silicon atom forms four equivalent sp^3 hybrid orbitals by mixing the s and all three p orbitals of its outer shell. This results in four unpaired electrons and the directions of four equivalent sp^3 hybrid orbital form tetrahedral angles of 109.4 degrees with each other. Silicon and Carbon atoms bond as a result of their HALF-FILLED sp^3 hybrids overlapping; and atomic bonding geometry will be tetrahedral in space because of the formation of FOUR sp^3 hybrid orbital directions.

2.4 SiC Network

The SiC crystal is made up of a network of tetrahedrally bonded silicon and carbon atoms. Each silicon atom is bonded to four carbon atoms as nearest neighbors and has twelve silicon atoms (no bonding) as second nearest neighbors and vice versa.

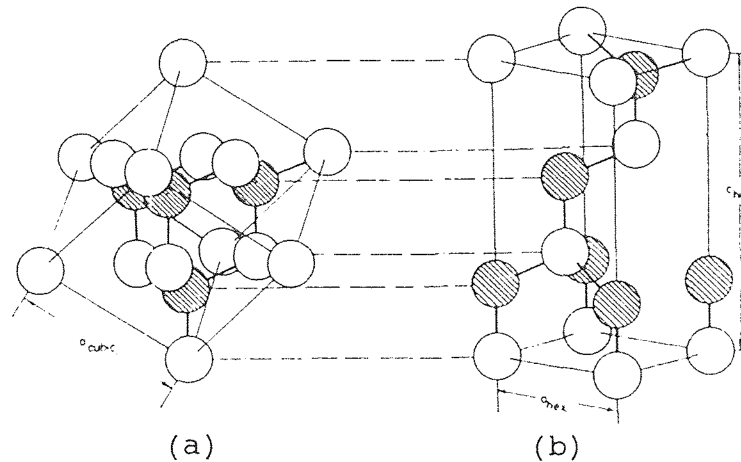

Figure 2.1 Zincblende structure with cubic and hexagonal unitcell

The unit cell of this binary tetrahedra structure could be either cubic, hexagonal or rhombohedral depending on the close packing stacking sequence. The cubic description is not advantageous if one desires to demonstrate the geometrical relationship between different tetrahedral structure types[4]. A unit cell transformation from cubic to hexagonal structure can be performed as seen in Figure 2.1. The arrangement of the atoms remains unchanged but a different translation pattern is chosen. The former cubic cell diagonal has now become the hexagonal c-axis.

The SiC structure consists of alternative single planes of Si atoms over single planes of C atoms with each Si atom directly above a C atom (Figure 2.1b). The many polytypes of SiC differ from one another only in the stacking sequence of such double layers (Figure 2.2b). Each successive double layer is stacked on the previous double layer in a close packed arrangement that allows

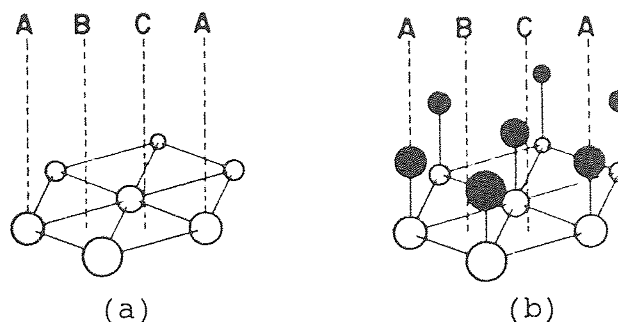

Figure 2.2 Structural unit slabs of (a) close packed element structure types. (b) Binary tetrahedral structure types.

for only three possible relative positions for the double layers. These positions are normally labeled A, B, and C as shown in Figure 2.2b. Depending on the stacking sequence, various structures such as cubic, hexagonal, or rhombohedral are produced.

The coordination tetrahedral in SiC are almost exactly regular [2]. Thus all SiC polytypes have hexagonal unit-cell dimensions of

$$a = 3.078\ \text{Å}, \quad c = n \times 2.518\ \text{Å}.$$

where n is the number of layers after which the stacking sequence repeats itself and is known as the identity period. The SiC bond length is given by

$$p = 3/4 \times 2.518 = 1.888\ \text{Å}.$$

2.5 Ramsdel Notation

In table 2.1 Ramsdel notation is used for some of the SiC polytypes. This notation represents a polytype by the number of layers in the unit cell and the letter H or R specifies the lattice type. A symbol nH represents a structure with an n-layered repeat period along c and a primitive hexagonal lattice, while mR denotes a structure with an m-layered repeat period along c and a lattice whose primitive unit cell is rhombohedral. This simple designation uniquely distinguishes each polytype except when two types have the same lattice as well as the same repeat period along c and differ only in the stacking sequence of the layers in their unit cell. Subscripts a, b, c, etc., are attached to the letter denoting the lattice type in such cases.

2.6 Some Explanations for Polytype Formation

The following explanations[2,4] have been offered to account for the occurrence of the different SiC modifications. However none has been able to explain all the observed structures.

1. Impurities present during growth.
2. Accretion of polymers of SiC with a stacking reversal inherent in their structure and stability governed by temperature.

3. Influence of a neighboring crystal with an orientation different from that of the growing crystal.
4. Spiral growth from screw dislocations.
5. Layer transposition caused by vibration entropy.
6. The electron energy configuration.

Table 2.1 Some of the known SiC polytypes

Ramsdel Notation	Hexagonal Cell		Rhombohedral Cell	
	a(Å)	c(Å)	a(Å)	α
2H	3.076	5.048	-	-
3C = (3R)	(3.08)	(7.55)	(3.08)	(60°)
4H	3.076	10.04	-	-
6H	3.080	15.09	-	-
8H	3.079	20.147	-	-
10H	3.079	25.13	-	-
15R	3.080	37.81	12.73	13° 53.5′
16H			-	-
18H			-	-
19H	3.079	47.84	-	-
21R	3.079	52.89	17.71	9° 58′
24H			-	-
27R	3.079	67.99	22.73	7° 46′
27H	3.079	67.99	-	-
33R	3.079	83.10	27.75	6° 21.5′
33H			-	-

Table 2.1 (Continued)

Ramsdel Notation	Hexagonal Cell		Rhombohedral Cell	
	a(Å)	c(Å)	a(Å)	α
$36H_a$	3.078	90.65	-	-
$36H_b$	3.078	90.65	-	-
39R				
39H			-	-
48H			-	-
$51R_a$	3.079	128.43	42.84	4° 07′
$51R_b$	3.079	128.43	42.84	4° 07′
54H			-	-
57R	3.078	143.52	47.88	3° 42′
66H			-	-
72R				
75R	3.079	188.87	62.98	2° 48′
78H			-	-
84R	3.079	211.54	70.53	2° 30′
87R	3.079	219.09	73.05	2° 25′
90R	3.078	226.6	75.42	2° 20′
95H			-	-
105R	3.078	264.39	87.98	2°
111R	3.078	279.5	93.18	1° 54′
120H			-	-
126R				
141R	3.079	355.04	118.36	1° 30′
168R				
174R				

Table 2.1 (Continued)

Ramsdel Notation	Hexagonal Cell		Rhombohedral Cell	
	a(Å)	c(Å)	a(Å)	α
192R				
273R				
351H				
393R	3.079	989.61	329.87	0° 32′
400H			-	-
594R				

Source: Parthe, E. Crystal Chemistry of Tetrahedral Structures. New York: Gordon and Breach, p112-115

No substance appears to show such a large number of stable and ordered polytypes as SiC. Table 2.2 in appendix 2 represents the most common SiC polytypes.

CHAPTER 3

PREPARATION METHODS

3.1 Historical Overview of SiC Research

"Carborundum" which is now the trade name of SiC is a blue crystal which was obtained by Acheson[5,6] as he was trying to crystallize carbon by disolving it in aluminum silicate in an electric arc. The word carburandum is synthesized from carbon and corundum (Al_2O_3) indicating its hardness to lie between that of the diamond and corundum. Prior to mid 1950's, SiC was produced for grinding and cutting purposes only by Acheson method. The initial research was limited to crystal structure and optical studies[1].

The importance of SiC as a high temperature semiconductor and the sublimation lely[7] process which was developed in 1955 to produce α-SiC crystals, increased the level of research for the next 15 years. At that time there were difficulties with this method. The uncontrolled nucleation resulted in formation of various polytypes (75% 6H,15R,4H) which in turn created a region of one dimensional disorder (transition region between adjacent polytypes). Such a disorder produces undesirable heterojunctions that is typical of all crystals with multiple polytypes[1]. A different method known as solution growth method[8,9] produced small ß-SiC crystals with very good electrical properties, but the results were not satisfactory.

Despite some progress, the main obstacle to SiC development was the lack of a reproducible crystal growth method[1]. As a result, except for fundamental investigations of optical properties at Westinghouse, SiC research ceased in the USA for the remainder of the 1970's.

The growing demand for high temperature electronics reinstated the SiC research in 1980's. Today the two leading crystal growth processes are the heteroepitaxial growth of large area ß-SiC on silicon substrate by CVD[10] (1982) and the Seeded-growth sublimation process[11] (1987).

3.2 Growth Methods

3.2.1 Conventional Methods

3.2.1.1 Acheson[2] Method

The process consists of fusing a mixture of carbon and silica, with a few percent of sawdust and common salt, in an electric furnace. The composition of the mixture may be, for instance, coke 40%, silica 50%, sawdust 7%, and common salt 3%. The furnace is not usually shielded from air, and employs a centrally mounted core of graphite and coke as the electrical heater element. The reaction mixture is filled around this core, between removable walls. The temperature of the central core is first raised to about 1900 °C, after which it is more slowly increased to reach a maximum value of about 2700 °C. The temperature is then lowered and maintained a little over 2000 °C for about 30 hours, after which the furnace is allowed to cool down and the silicon

carbide removed, washed, dried and graded according to size. The best grades are found near the core. The exact temperature-time cycle varies from furnace to furnace, depending on its geometry.

While the reaction is estimated to be completed at 1800 °C, the SiC produced is in the form of a fine yellow-green crystalline powder unsuited for grinding purposes. The SiC from colder parts of the furnace, which do not reach 1800 °C, is white and has a frosty appearance. The form in which SiC can be used commercially is produced by the recrystallization of this material by the further heating at temperatures above 2000 °C. When the temperature of the core is raised to 2700 °C, the SiC formed close to it is decomposed, liberating Si which reacts with the C in the colder parts of the furnace. A residue of graphite is left around the core, surrounded by a hard crust of SiC. The shrinking of the sawdust keeps the mixture porous and promotes the circulation of the reaction gases, making it possible for the large amounts of CO evolved to escape smoothly. The common salt reacts with the impurities present to form volatile chlorides which escape, thereby improving the purity of the product.

3.2.1.2 The Method of Gaseous Cracking

It is interesting to note that the wurtzite form of Sic (type 2H) which has not so far been found in any of the commercial samples, has been grown by this method.[2]

Small transparent cubic SiC crystals have been deposited on heating (above 2000 °C) filaments of C, ZrC and TaC, (in place of tungsten) in a gas mixture of $SiCl_4$, Toluene ($C_6H_5CH_3$) and hydrogen[12]. Other gas sources such CH_3SiCl_3 with hydrogen have produced very small 300 μ ß-SiC at 2400 °C.

3.2.1.3 The Method of Sublimation (Lely method)

Lely[13] has devised a method of obtaining pure SiC from the technical grade by a process of sublimation and condensation. For an appreciable sublimation of SiC it was necessary to suppress the dissociation of the compound. This was accomplished by constructing a pseudo-closed vessel in which the pressure of the most volatile component would be equal to the pressure of this component in the normal dissociation equilibrium at a certain temperature.

A hollow cylinder constructed from lumps of technical-grade SiC was heated to a temperature of 2500 °C in a carbon crucible. The SiC cylinder was closed by a large lump of SiC and the temperature regulated to be highest at the outside, and also higher in the middle than at the top and the bottom. When heating was continued for a number of hours, new separate crystals were found to have grown on the lumps

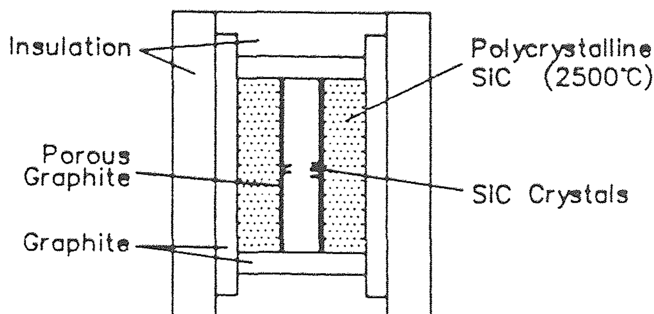

Figure 3.1 Growth cavity used in the sublimation (Lely) process

on the inside of the cylinder, while dense layers of SiC were deposited on the top and the bottom. Since the sublimation is carried out at the temperature of over 2500 °C, the resulting crystals are always of the high-temperature α-SiC modification. All polytypes obtained by this method were reported by Lely to be hexagonal and were presumably of type 6H; but Knippenberg[14] has found among them types 4H, 8H, and 15R as well as some other long-period polytypes.

3.2.1.4 The Method of Crystallization from Solution

Carbon has an appreciable solubility in silicon, at a temperature of about 1700 °C. Therefore, SiC crystals can be grown from a C-rich Si melt (at 1700 °C), the solution being supersaturated with respect to SiC[2].

Only the cubic form of SiC (ß-SIC) is produced by this method. It is, however, difficult to draw or grow good SiC crystals from the solutions. The crystals obtained are small and tend to grow in polycrystalline agglomerates.

3.2.2 Recent Methods

3.2.2.1 The Modified Sublimation Process

The original Lely method produced platelet monocrystals. From 1955 to 1980, these platelets were used for fundamental investigations.[15]

However, to grow 6H-SiC ingots large enough to be technically useful as substrate material, the best way is the sublimation growth method with controlled deposition of SiC on a seed crystal in a temperature gradient, the modified Lely method[16,17,18]. The three essential parameters for crystal growth are growth temperature, temperature gradient, and pressure inside the reaction chamber. A negative temperature gradient of 10 to 25 °C/cm^{-1} towards the seed crystal is adjusted in contrast to the conventional Lely method. The growth temperature together with the polytype and the orientation of the crystal used mainly determines the polytype of the growing crystal, whereas temperature gradient and gas pressure control the transport and hence the crystal growth velocity.

Nucleation takes place on a SiC seed crystal located at one end of a cylindrical growth cavity[18]. A temperature gradient is established within the cavity such that the polycrystalline SiC is at 2400 °C and the seed crystal is at 2200 °C. At these temperatures SiC sublimes from the polycrystalline material and condenses on the cooler seed crystal. Growth takes place on the seed crystal in an atmosphere of argon at 200 Pa. Large boules of single

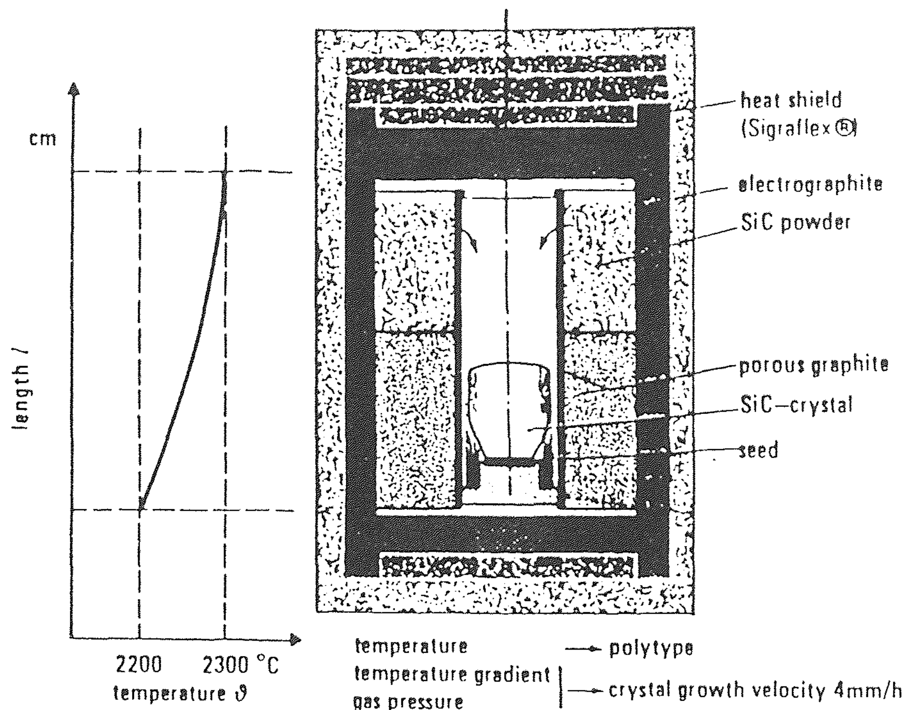

Figure 3.2 Crucible assembly for the growth of SiC single crystals by the modified Lely method.

polytype 6H SiC are grown with growth rates of about 4 mm/h and boule sizes up to 20 mm in diameter and 24mm long.

At NCSU, 6H SiC single crystals, 15mm in diameter and 8mm thick, have been grown by this seeded-growth sublimation process[11]. Unintentionally-doped crystals are transparent and colorless; nitrogen-doped crystals are green. Preliminary **TEM** studies indicates a much lower density of line and planar defects (compared to SiC grown on Si).

3.2.2.2 Heteroepitaxial Growth of SiC by CVD

Growth takes place in a fairly conventional horizontal CVD system[19,20]. The Si substrates are supported and heated by an rf-heated graphite susceptor. Hydrogen is the carrier gas and flows continuously during the process. Other gases are added for various steps.

In the first step, HCl is added for two minutes with the Si substrate at 1200 °C to chemically remove about 2μ of the Si surface. This provides a good surface for the next step, the growth of the initial SiC layer. The essential element of this step is a rapid temperature ramp from near room temperature to the growth temperature in the presence of a hydrocarbon. To prepare for this step, the suceptor and the substrate are allowed to cool for several minutes after the HCl etch. When near room temperature is reached, C_3H_8 is added to the carrier gas. After allowing an additional 30 seconds for the flow equilibrium, the temperature of the suceptor and substrate is ramped to 1360 °C in about 30 seconds. The C_3H_8 is left on for an additional 90 seconds and then turned off. During the 2 minute period (ramp plus 90 seconds of additional growth), a single crystal ß-SiC film, about 20 nm thick, is produced on the Si substrate. After a two-minute purge with the H_2 carrier gas, SiH_4 and C_3H_8 are added to initiate the final step, the bulk growth of ß-SIC to the desired thickness. A typical 3-hour run yields a 10 μm ß-SiC single crystal film on the Si substrate. The orientation of the film is the same as the

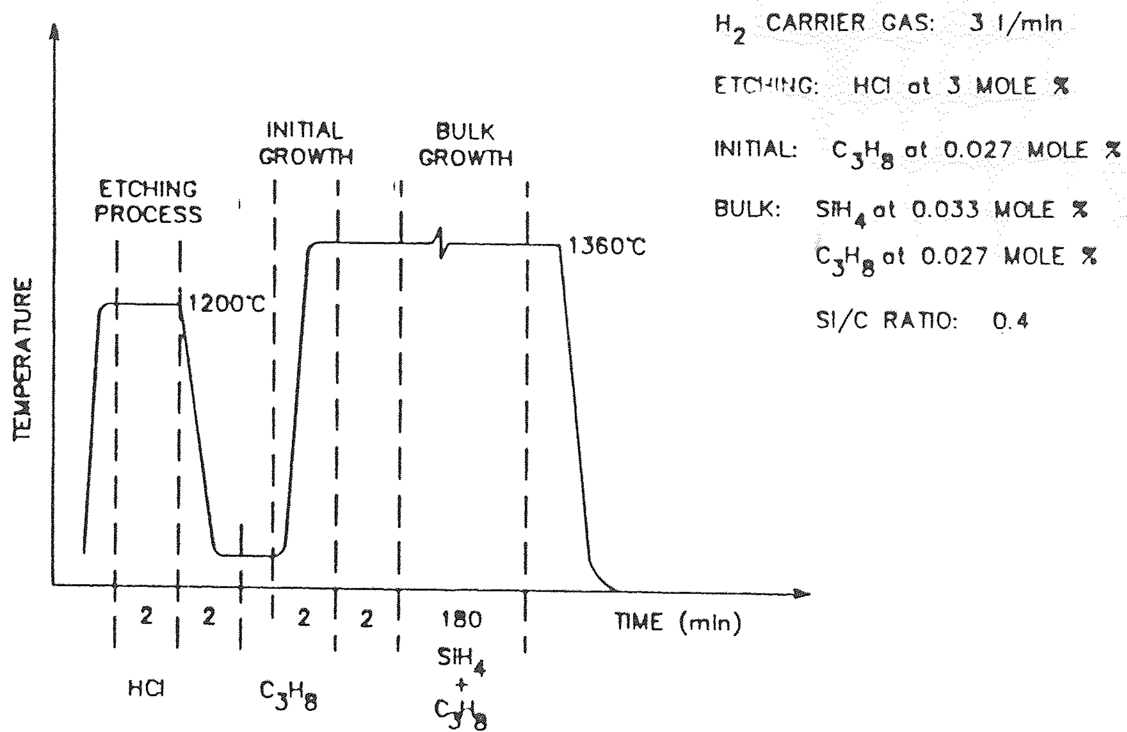

Figure 3.3 Process steps for growing ß-SiC on Si

substrate. A (001) substrate orientation is preferred because the (111) orientation produces films that are severely warped and cracked.

3.2.2.3 Plasma Enhanced CVD of a-SiC:H

Plasma assisted chemical vapor deposition (PECVD) consists of the techniques of forming solid deposits by initiating chemical reactions in a gas with an electric discharge.[21]

PECVD is a highly complex chemical process. The discharge produces a wide variety of chemical species, free radicals, electrons and ions, and it can also induce chemical changes at the surface of the growing film. Modeling is impaired not only by the fact that the most important physical and chemical processes have not been singled out, but also by the ignorance of boundary conditions.

The main advantage of plasma CVD over thermal CVD is the ability to deposit films at relatively low substrate temperatures (typically less than 300 °C). Instead of requiring thermal energy, the energetic electrons in the plasma can activate almost any reactions among the gases in the discharge. At the same time, the bulk of the gas and the substrate do not reach high temperatures because of the non-equilibrium nature of the glow discharge plasma.

As a result, CVD films, which are mismatched in thermal expansion coefficient with the substrate, can be deposited with plasma assistance without severly stressing the film upon cooling to room temperature. Also high temperature CVD processes are often unacceptable for deposition over other films or structures which would either vaporize, melt, flow, diffuse or undergo a chemical reaction. Another advantge is

that at reasonable or acceptable temperatures, PECVD often has much higher deposition rates than conventional thermal CVD.

The major limitation of PECVD is that deposition of pure materials is virtually impossible. Because of the reduced substrate temperatures, desorption of product gases is ineffective resulting in the incorporation of these elements in the film. For example, amorphous silicon deposited from silane is heavily hydrogenated. However, as in the case of hydrogenated amorphous silicon for solar cells, this can be an advantage. Another major disadvantage is the strong interaction of the plasma with the growing film.

Plasma Enhanced CVD has many process variables such as power, frequency, powered or grounded substrates, pressure, cathode/anode spacing, substrate temperature, gas flows and flow ratios. While the number of variables makes a process complicated, it allows a process to be adjusted for control of film properties. Thus, it is necessary to understand the deposition mechanism in detail in order to produce films with desired properties. In general the deposition mechanism of PECVD processes can be divided into four major steps[22] as follows:

(1) The primary reactions between electrons and reactant gases in the plasma to form a mixture of ions and free radical reactive species.

(2) The transport of reactive species from the plasma to the substrate surface in parallel with various secondary inelastic and elastic reactions, e.g., ion-radicals, photon-molecules, etc. Steps 1 and 2 occur in plasma glow discharge and sheath region, and can be classified as radicals and ion generation steps in plasma[23].

(3) The reaction or absorption of reactive species (radical absorption and ion incorporation) with or onto the substrate surface.

(4) The rearrangement processes where reactive species or their reaction products incorporate into the growing film or re-emit from the surface back into the gas phase. Step 3 and 4 involve various heterogeneous reactions and interactions between ions and radicals with the surface in the sheath region.

Steps 3 and 4 generally have a critical effect on the final film properties.

CHAPTER 4

PROPERTIES

4.1 Electrical Properties

4.1.1 Review of Prior Hall and Related studies on SiC

Hall coefficients and resistivities of heteroepitaxial ß-SiC films deposited on Si (100) by CVD have been measured by several groups of investigators[24]. Sasaki et al.[25] analyzed the carrier-concentration data obtained on undoped films as a function of temperature (300-1100 K) using the assumption that the shallow donors were not compensated [$n \sim \exp(-E_D/2kT)$]. They obtained an ionization energy E_D for the primary donors of 40-50 meV. Good agreement with the values for N determined by photoluminescence (PL) measurements[26,27] was claimed. Similar research within the temperature range 4-300 K and a more detailed analysis by Segal et al.[28,29] revealed that their undoped films were highly compensated (the ratio of the concentrations of acceptors and donors, $N_A/N_D > 0.9$). Moreover, the donor ionization energies were 13-17 meV or less than one-half the values conventionally reported without the assumptions of compensations. They argued that applying the compensation model [$n \sim \exp(-Ed/kT)$] was reasonable due to the better fitting of the theoretical curve to the experimental data. They examined the relation between E_D and N_D empirically established for intensively studied semiconductors such as

Si, Ge and GaAs. From the good fit of their data to the data obtained by Aivazova et al.,[30] in which the presence of N was confirmed by **ESR**, it was also claimed that N was the origin of the shallow donor in the ß-SiC films. Curve fitting of the theoretical equation (1) to data determined by Yamanaka et al.[31] for the variation of carrier concentration with temperature (10-1000 K) also showed heavy compensation with N_a/N_d > 0.9 and a donor ionization energy of 18 meV in the undoped films. Contrary to the opinion of Segal et al.,[28,29], these latter authors doubted the presence of N in their films because of the very low partial pressure of this species in the reactant system. Instead, it was suggested that the structural defects such as antisite atoms or vacancies behave as shallow donors. Suzuki et al.[32,33] have conducted Hall measurements on both undoped and N-doped films within the temperature range of 70-1000 K and calculated values of N_A and N_D from the carrier-concentration data. Their films were also highly compensated (N_A/N_D>0.9 for the undoped samples, N_A/N_D~0.8 for the N-doped samples). These investigators also doubted the presence of N in their undoped films and referred to the origin of the shallow donors as being "unknown." For the undoped films, the value of E_d was 20-22 meV and thus similar to that reported in the other Hall measurements. However, the ionization energies of N-doped films calculated from these measurements were 5-16 meV. Subsequently, they theoretically analyzed the electron Hall mobility versus

temperature data from the same measurements[34]. The results of this analysis showed the donor and acceptor concentrations and the degree of compensation, N_A/N_D, to be significantly different from their values determined from carrier-concentration versus temperature data. The donor and acceptor concentrations were in the range of 10^{16} cm^{-3}, contrary to the values of 10^{17}-10^{18} cm^{-3} from the analysis of the temperature dependence of the carrier concentration. The degree of compensation in the undoped films decreased to as low as 0.45, while that in the N-doped samples as determined to be 0.33-0.40. It was claimed that the mobility-versus-temperature analysis has an advantage due to its sensitivity in determining parameters. It was also proposed[34] that their theoretical calculations of the electron mobilities based on the results of the analysis[32,33] of the carrier-concentration versus temperature data did not yield values consistent with the experimentally measured values. Moreover, they claimed[34] that the measured values of electron Hall mobility from their carrier-concentration versus temperature data are too high based on the theoretical curve of van Dall[35] extrapolated to the mobility of 1300 $cm^2/(V\ s)$ for a pure, defect-free ß-SiC, and considering the donor and acceptor concentrations in their films obtained by their analysis.[32,33] However, many assumptions inherent in the choice of the scattering mechanism were used in fitting the theoretical lines to the mobility data. Multiple

contributions of different scattering processes would make the analysis even more difficult.

The shallow-donor ionization energy range of 13-22 meV has been consistently obtained, even though there is disagreement regarding the origin of these levels. These data have resulted in a close examination of the **PL** spectra and related information for the ß-SiC films. Carlos et al.[36] conducted **ESR**, **PL**, and Hall measurments on these films. The **ESR** (25-200 K) and **PL** (1.5-120 K) measurments detected the presence of N as a donor with a binding energy of 53 meV. No other shallow donors were detected by these techniques. From their Hall data, they reached similar conclusions as the previous investigators in that (1) a donor ionization energy of ~20 meV exists and (2) high levels of compensation exist in the films. After examining the **PL** spectra at 1.5 K, Freitas et al.[37] subsequently noted that the donor ionization energy level of 13-22 meV may come from N if it is spatially inhomogeneously distributed in the film. It should be noted that **PL** is not applicable for the determination of energy levels which do not undergo photoemission processes.

Finally, a related theoretical study of the dominant point defects in ß-SiC as a function of composition and the Fermi-level position has been conducted by Wang, Berholc, and Davis.[38] In the case of n-type, Si-rich ß-SiC (which is the usual type of undoped ß-SiC), the Si antisite atoms are the dominant defects with the second most abundant

defects being the C vacancies. This result supports the Si self-diffusion model involving Si antisite atoms and C vacancies proposed by Birnie.[39] However, the Si antisite atoms are electrically inactive and the C vacancies are double donors. This does not explain the high concentration of compensators in ß-SiC films on Si (100) described above. There is, however, the possibility that the Si antisite atoms (or other defects) act as compensating species such as electron traps. Thus, no conclusion has been reached regarding the origin of the shallow-donor levels of E_D = 13-22 meV in ß-SiC films grown on Si (100).

4.1.2 Temperature Dependence of Electrical Properties of ß-SiC Grown by CVD

3C-SiC is expected to be an excellent material for electronic devices operated at high temperatures because of its wide band gap (2.2 eV) and high electron mobility (~1000 cm^2 V^{-1} s^{-1}) compared to that of silicon[25]. Few papers have been published on the high-temperature electrical properties of 3C-SiC. Van Daal[40] has studied the temperature dependence of electrical properties of 3C-SiC crystals prepared by the Lely method. However, the crystals had very poor electrical properties compared with those of 6H-SiC and 15R-SiC. On the other hand, though the crystals grown from carbon-saturated silicon melts have large electron mobilities (~1000 cm^2 V^{-1} s^{-1}), the crystals obtained were very small (~1 mm^2) and inhomogeneous.[2]

Nishino et al.[3,4] obtained single crystals of 3C-SiC, having large area of 22 X 50 mm^2 epitaxially grown on Si by chemical vapor deposition (CVD). They used a buffer layer made by carbonizing the Si surface to release large lattice mismatch between SiC and Si (about 20%), and obtained epitaxial layers with good electrical properties.

Following sections are brief reports about this topic by several groups.

4.1.2.1 K. Sasaki et al (1984)

They [25] reported the electrical properties of 3C-SiC epitaxial layers on Si, prepared by CVD, at temperatures between room temperature and 850 °C, and showed that because of its large electron mobility at high temperatures compared with other polytypes, 3C-SiC was a useful material for devices operated at high temperatures.

3C-SiC was epitaxially grown on Si (100) substrates of 10 X 10 mm^2. Growth rate was about 2.5 $\mu m/h$ and the thicknesses were in the range between 6 and 20μm. (RHEED) analysis indicates that the grown layers were single crystals of 3C-SiC and the (100) plane of SiC is parallel to the substrate surface.

The electrical properties of the epilayers were studied using the van der Pauw method[41] at temperatures between room temperature and 850 °C. Prior to the measurments, Si substrates were removed by chemical etching. Four nickel electrodes of 1-mm diameter were deposited on the epilayers

and Ohmic contacts were achieved by annealing in Ar atmosphere at 1050 °C for 3 min. Hall measurments at high temperatures were carried out in vacuum of 10^{-6} Torr.

All the epilayers obtained show n-type conduction. The carrier concentration ranges between $5X10^{17}$ and $1X10^{18}$ cm^{-3}, and the Hall mobilities between 120 and 200 $cm^2/V.s$ at room temperature.

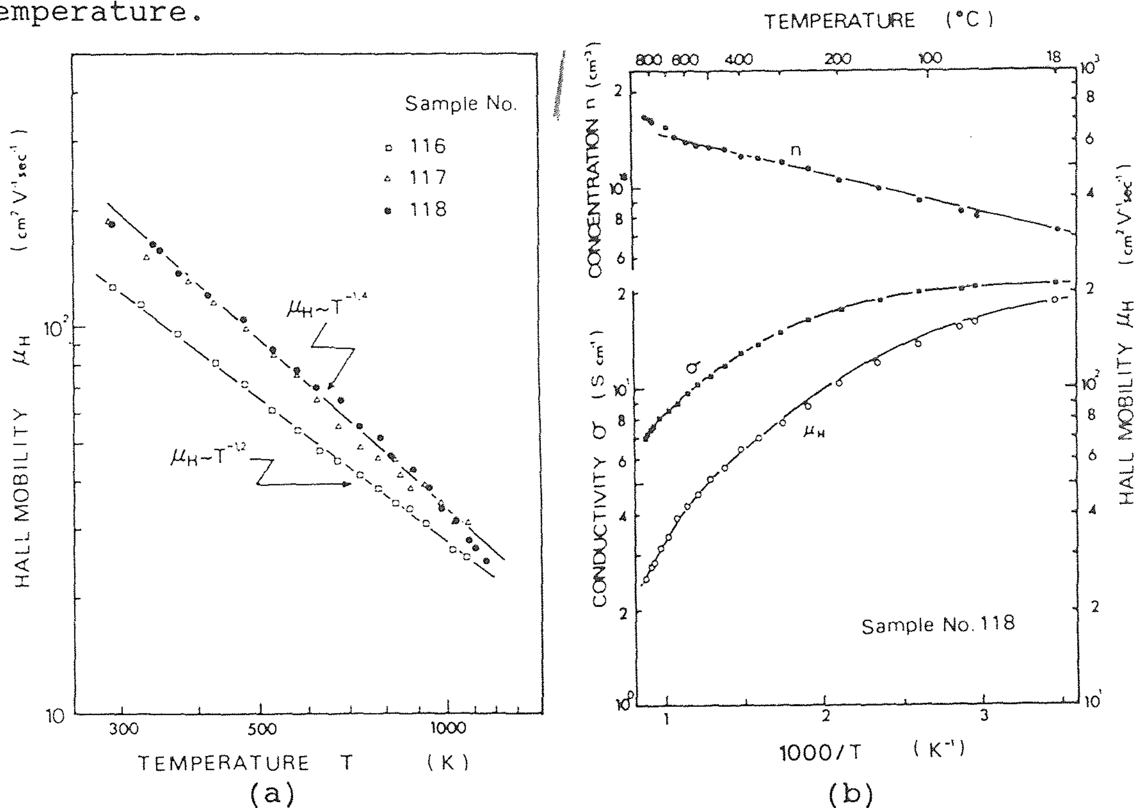

Figure 4.1 (a) Hall mobilities μ_H of three samples of 3C-SiC epilayers as a function of temperature. (b) Temperature dependence of conductivity σ, Carrier concentration n, and Hall mobility μ_H of a 3C-SiC epilayer.

In Figure 4.1a, the Hall mobilities of three samples are shown as a function of temperature. The values of the mobilities plotted in the figure were calculated neglecting the correction of the scattering factor. In the

temperature region between 400 and 500 °C, the mobilities range from 40 to 60 cm^2/V.s. The temperature dependence of conductivity σ, carrier concentration n, and Hall mobility μ_h are shown in Figure 4.1b. All the samples investigated have negative temperature coefficients of conductivity above room temperature. At 800 °C, the mobilities decrease to 20-30 cm^2/V s. The values of α in the relation [$\mu_h \sim T^{\alpha}$], determined from the slope of log μ_h vs. log T plots, are between -1.2 and -1.4.

The values of α for other polytypes (6H, 15R, 4H) have been reported as between -2.0 and -2.6 in this temperature range[42,43] except for highly doped samples, and the mobilities decrease more steeply with increasing temperature as compared with those of 3C-SiC. In the case of 6H-SiC and 15R-SiC, it is considered that the electron mobility at high temperatures is restricted by intervalley scattering as well as acoustic phonon scattering[42,44], which results in the steep decrease of mobility with increasing temperature. On the other hand, in the case of 3C-SiC, the mobility is little affected by intervalley scattering because of its crystal symmetry[45]. Therefore, it is anticipated that the value α of 3C-SiC is smaller than those of other polytypes and its mobility is large even at high temperatures. They[25] pointed out that their results of the value of α = - 1.2~ - 1.4 supports this assumption, and it is considered that, in 3C-SiC, acoustic phonon scattering prevails in the scattering processes for this temperature range.

The small value of α is of great advantage to high mobilities at high temperatures. In fact, though the mobilities of our samples are smaller than those of other polytypes at room temperature, at the temperature above 500 °C, the mobilities of our samples are larger.

4.1.2.2 B. Segall et al. (1986)

Hall measurments on four n-type cubic SiC films epitaxially grown by chemical vapor deposition on (100) Si substrates are reported[28]. The samples investigated were prepared on p-type Si substrates by the method described earlier[10]. All samples were roughly square with sides approximately 5 mm and thicknesses from 4.6 to 16.9 μm. Electrical contacts were made on each corner, in a square pattern and 2.5mm apart, by sputter deposition of Ta/Au.

Measurments of the resistivity and Hall coefficient were made with dc current using the van der Pauw technique [41]. Magnetic fields up to 13kG were used. The temperature was varied in a gas flow cryostat and stabilized to within 0.02 K.

The carrier concentrations n(T) were obtained from the Hall coefficient R_H by [$n = 1/(R_H e)$]. Experimental results for three of the four samples studied are shown as points in Figure 4.2a. One of the samples (number 438), which was fairly thick (16.9 μm) and hence capable of being separated from the substrate, was also subjected to high-temperatures ($300 K < T < 800 K$). Results for this sample are shown in

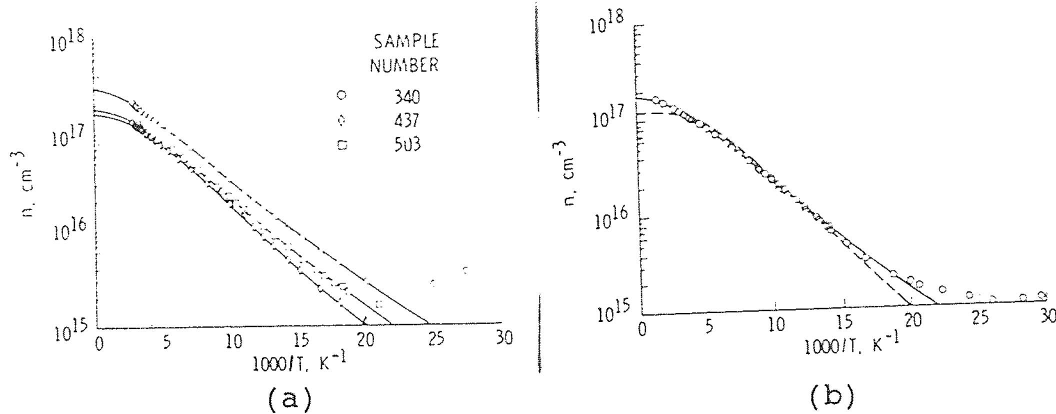

Figure 4.2 Carrier concentration n vs. 1000/T. The points are experimental results [28] while the continuous and dashed lines are calculated fits using compensation and noncompensation, respectively. (a) Three cubic SiC samples. (b) a self-suporting sample.

Figure 4.2b. As some measure of the quality of the samples, we note that the room-temperature mobilities for sample numbers 340, 437, 438 and 503 are 270, 310, 305, and 245 cm^2/V s, respectively. Here they[28] use the appropriate relation

$$n(n+N_A)/N_D-N_A-n = N_C/s \exp(-E_D/kT) \qquad (4.1)$$

which is accurate for a single level and nondegenerate carriers. The fitting of n(T) is obtained by a linearized least-square fit[46] with E_D, N_D, and N_A as variables. The values for E_D N_D, yielding these curves are given in table 4.1.

The first point evident from the tabulation is that the samples are highly compensated with $N_A/N_D > 0.9$. The second is that the values of E_D are much smaller than the published

Table 4.1 Parameters and errors estimates obtained in a linearized least-squares fit using a compensated model.

Samples	N_D (10^{18} cm^{-3})	N_A (10^{18} cm^{-3})	E_D (meV)	No. of points
340	2.61±0.15	2.32±0.15	13.7±0.2	23
437	1.76±0.09	1.60±0.09	17.1±0.2	24
438	1.77±0.09	1.61±0.08	15.2±0.2	28
503	2.15±0.12	1.97±0.12	14.7±0.2	28

Source: Segall B. et al. Appl. Phys. Lett. 49 (1986): 584.

film values (less than one half) and the generally accepted values for the nitrogen donor (50 meV). Another point evident in the tabulation is the variation of E_D with N_D. In figure 4.3, they[28] plot all the energies, E_D, versus N_D. Aside from some scatter, the E_D points lie on a curve which extrapolates to the value of the nitrogen donor at N_D = 0 and vanishes at $N_D = N^{-}_D$, slightly above those of their samples.

Such a curve can be represented by the relation used for shallow acceptors in Si[48] and shallow donors in Ge,[49]

$$E_D\ (N_D) = E_D\ (0) - \alpha\ N_D{}^{1/3} \qquad (4.2)$$

In the effective mass approximation, they find $N_D = 10^{19}$ cm^{-3}. This agrees satisfactorily with the value $6.3X10^{18}$ cm^{-3} indicated by the curve. They[28] claim that the magnitude of $E_D(0)$ agrees satisfactorily with the accepted value of nitrogen donor at the dilute concentration[26]. Aivazova et al.[30] have identified their donors as nitrogen

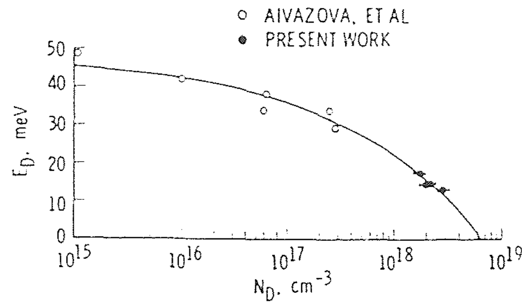

Figure 4.3 Donor activation energy E_D vs donor density N_D. The continuous line is given by Eq. (4.2) using $E_D(0)=48$ meV and $\alpha=2.6X10^{-5}$ meV cm.

by electron spin resonance (**ESR**) measurements. The above correlations suggest the same identification for the donors in their samples. Considering the preparation conditions for the present samples, nitrogen contamination seems reasonable.

In conclusion, Segall et al.[28] claim that a high degree of compensation and a large impurity concentration induced reduction of the donor depth in all samples.

4.1.2.3 M. Yamanaka et al. (1987)

Yamanaka et al.[31] reported the temperature dependence of the electrical properties of unintentionally doped n-type and Al-doped p-type 3C-SiC epilayers on Si grown by CVD, and provided information on activation energies of Al acceptors and residual donors and hole scattering mechanisms.

Single crystals of 3C-SiC were epitaxially grown on Si(100) substrates of 60X70 mm^2 by CVD. The thickness of the samples were in the range between 6 and 50 μm.

The electrical properties of epilayers were studied using the van der Pauw method at temperatures between 10 and 1000 K. The epilayers were cut into the size of 10 X 10 mm^2 and Si substrates were removed by Chemical etching. Four Ni and Al (89 wt %)-Si(11 wt %) electrodes of 1 mm diameter were deposited on the corners of n- and p-type epilayers, respectively, and ohmic contact was achieved by annealing at 930 °C in 10^{-6} Torr for 3 min. Hall and resistivity measurments were carried out at 10^{-6} Torr. The temperature of the samples were monitored by **CA** and **CR-AuFe** thermocouples for high (above 270 K) and low (below 270 K) temperatures, and controlled within ±0.5 and ±0.05 K. In the measurements, the effect of thermoelectric voltage caused by the inhomogeneity of temperature over the sample was eliminated by averaging the data obtained by reversing the current direction.

The SiC epilayers grown with no more than 3% of Al/Si ratio in the reaction gases are single crystals of 3C-SiC and the (100) plane of SiC is parallel to the substrate surface, according to the results of Reflection High-Energy Electron diffraction (**RHEED**) analysis.

All the unintentionally doped epilayers show n-type electrical conduction, and have a light yellow color. The carrier density n is 3-7X10^{16} cm^{-3}, and the Hall mobility μ_h, is 400-500 cm^2/V.s at room temperature. In figures 4.4(a) and (b), the carrier densities and the Hall mobilities of the unintentionally doped n-type samples are shown,

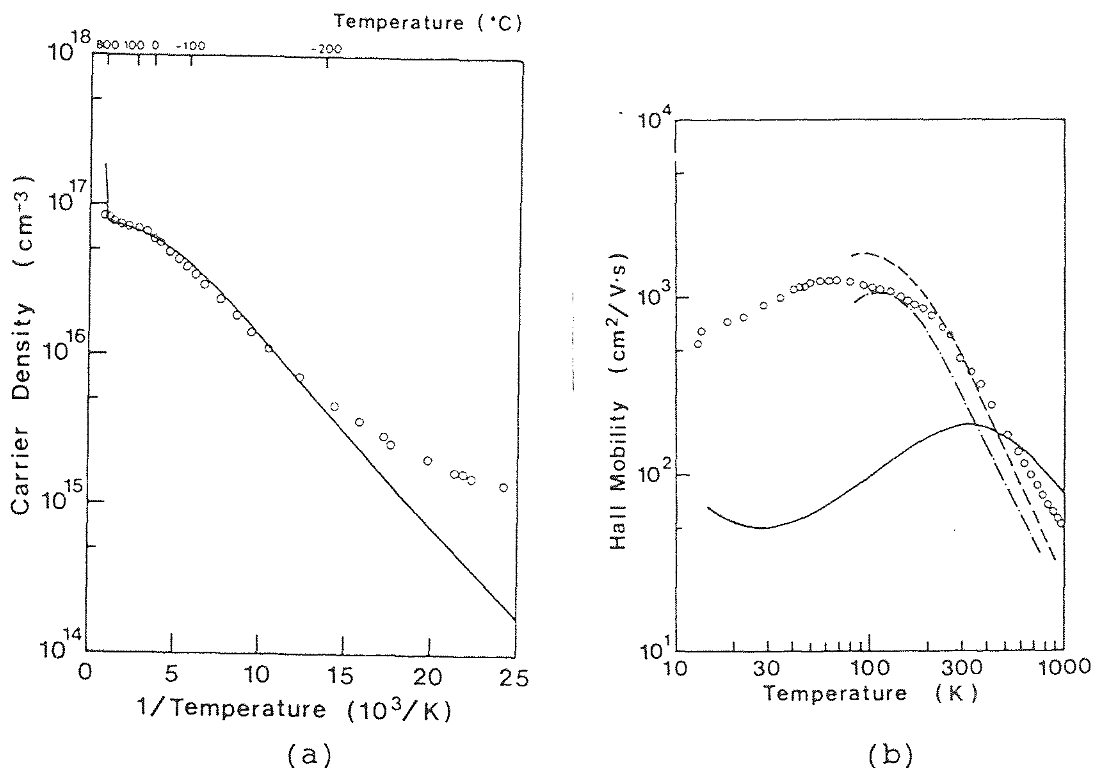

Figure 4.4 Temperature dependence of (a) carrier density and (b) Hall mobility of an unintentionally doped n-type 3C-SiC epilayer with calculated values denoted by a solid curve. Dashed and dot-dashed curves denote temperature dependencies of electron mobilities of 15R-SiC and 6H-SiC, respectively.

respectively, as a function of temperature. The carrier density decreases monotonically with decreasing temperature, and the Hall mobility has a maximum (~1000 cm^2/V.s) between 60 and 80 K and decreases with $T^{-1.8}$ dependence for increasing temperature.

In figure 4.5, the carrier densities and the Hall mobilities of the Al-doped epilayers are shown as a function of Al/Si ratio in the reaction gases. Electrical conduction in the Al-doped epilayers changes from n type (denoted by open circles) to p type (denoted by solid circles) through the high-resistivity region, and a green cast was introduced

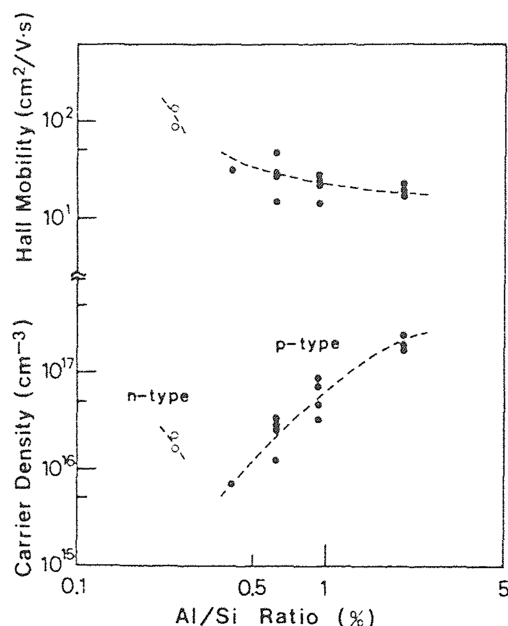

Figure 4.5 Al/Si ratio dependencies of carrier concentration and Hall mobility of Al-doped 3C-SiC.

with increasing Al/Si ratio. The p-type epilayers were obtained in the range between 0.4 and 3% of the Al/Si ratio. The carrier density p ranges between $1X10^{16}$ and $4X10^{17}$ cm^{-3}, and the Hall mobility between 40 and 10 $cm^2/V.s$ at room temperature. The epilayers at the upper stream side have higher carrier densities and lower Hall mobilities than those at the lower stream side. With an increasing Al/Si ratio of more than 3%, the coloration rapidly approaches gray with a cast of green and the measurement can not be carried out because of the high resistivity of the samples.

In figures 4.6a and b, the carrier densities and Hall mobilities of two typical Al-doped p-type samples are shown, respectively, as a function of temperature. The carrier density in the p-type samples decreases steeply with decreasing temperature, and the Hall mobility has a maximum

(~40 cm^2/Vs) at about 250 K, and varies as $T^{5.0}$ and $T^{-2.0}$ on the low- and high-temperature sides of the peak, respectively. The Hall mobilities in the p-type samples having different carrier densities also show a similar temperature dependence within the present experiment.

For the unintentionally doped n-type, they[31] obtained E_d = 18 meV, $N_D = 9.5X10^{17}$ cm^{-3}, and $N_A = 8.7X10^{17}$ from the fitting of the calculated carrier density to experimental results. The calculated carrier densities solid curve in figure 4.4(a) are in good agreement with the experimental results at the temperatures above 70 K.However, at temperatures below 70 K, they deviate from the experimental results, which depend slightly on temperature. This behavior, though not understood, is similar to the results in hexagonal SiC reported by other researchers[40,43]. The obtained value E_d = 18 meV is different from 40 to 50 meV obtained by Hall measurements of the n-type samples with n ~ $5X10^{17}$ cm^{-3} and μ_H ~ 200 cm^2/V s at room temperature[25], and from 53 and 38 meV obtained by photoluminescenece and electron cyclotron resonance measurements[44,27], respectively. Residual donors in 3C-SiC have been considered to be nitrogen impurities. However, those in highly pure 3C-SiC epilayers are thought to be not due to nitrogen impurities but due to structural defects, e.g., antisite atoms or vacancies, because of the different activation energy from nitrogen impurities and of very low partial pressure of residual N_2 in the reaction tube.

The differences between calculated and experimental electron mobilities in figure 4.4b were considered to be due to the following assumptions in the calculations[13].

(1) μ_H was assumed to be equal to μ. However, μ_H is usually larger than μ.

(2) All the acceptors were assumed to be ionized to compensate the donors in the calculation of carrier density. The carrier density might be underestimated at high temperatures, because reexcitation of electrons from the ionized acceptors to the conduction band is neglected.

(3) In figure 4.4(a), the calculated carrier density deviates from the experimental results, which depend slightly on temperature, below 70 K. This deviation suggests that the mechanism of conduction might change about 70 K, and the origin of the deviation must be taken into account in the calculation.

In the consideration of these factors, the densities of donors and acceptors, i.e., ionized impurities decrease to some degree, which results in the shift of the calculated value of mobility towards the experimental results. The reexcitation of the electrons could not be estimated quantitatively because of the lack of the information about the acceptor levels in unintentionally doped 3C-SiC.

For the two Al-doped p-type samples, the obtained parameters were E_a=160 meV, N_A=2.0X10^{19} and 5.5X10^{18} cm^{-3}, and N_D=5.o and 3.5X10^{18} cm^{-3}. The calculated values are also

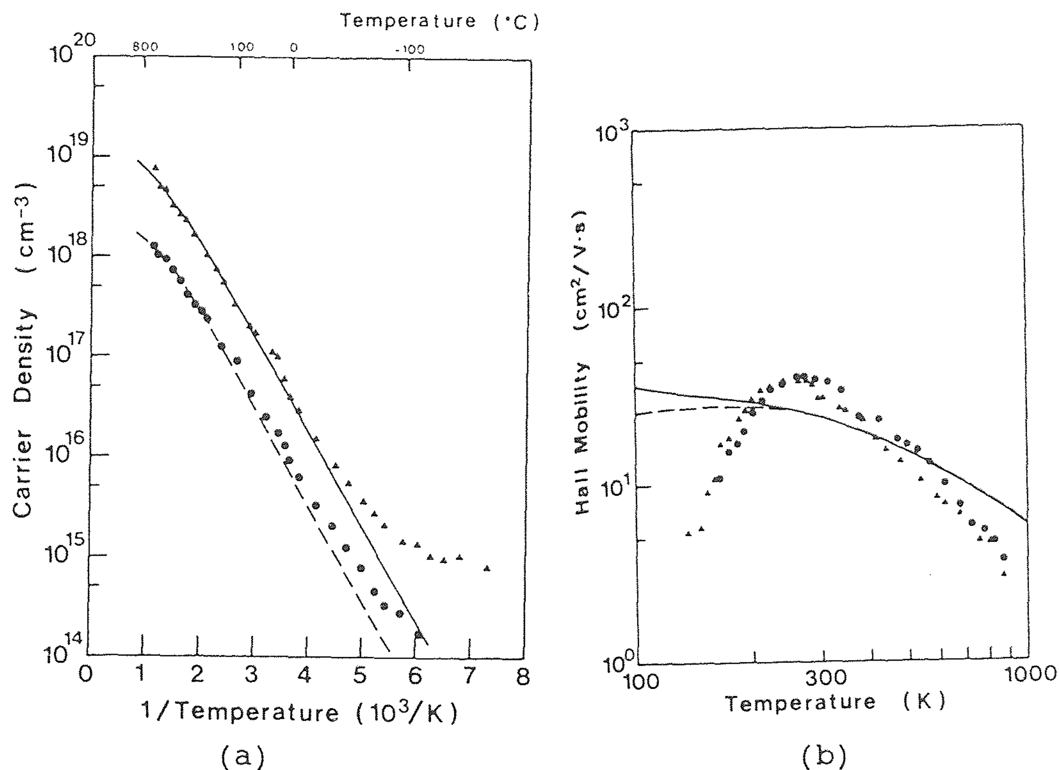

Figure 4.6 Temperature dependencies of (a) carrier densities (b) Hall mobilities of two Al-doped p-type 3C-SiC epilayers with calculated values denoted by solid and dashed curves.

plotted in figures 4.6a and b. The calculated carrier densities (solid and dashed curves) are in agreement with the experimental results, respectively, in figure 4.6a. The obtained value of E_a=160 meV is independent of the density of Al acceptors within the present experiment, and is different from 257 meV obtained from photoluminescence measurements[27]. The smaller value obtained may be attributed to the effect of the screening by the ionized impurities because of the high density of the ionized impurities. 40-60% of Al acceptors are compensated in the present samples. N_D in the p-type sample is much higher than that in the unintentionally doped n-type and N_D at the upper

stream side is higher than that at the lower stream side. These results suggest that the density of the structural defects is increased by adding Triethylaluminum (**TEA**) in the reaction gas system.

The calculated hole mobilities (solid and dashed curves) are not in agreement with the experimental results in figure 4.6(b)[31]. At the temperature where the calculated curves deviate, the dominant scattering mechanism is considered to be not acoustic phonon scattering but ionized impurity scattering. It is due to the same reason as in the case of the unintentionally doped n-type samples that the calculated values do not show $T^{1.5}$ dependence at low temperature. Therefore, the temperature where the mobilities become maxima is nearly equal between the experimental results and the calculated values, and hole mobility is considered to be dominantly limited by acoustic phonon scattering at temperatures above 300 K, and by ionization impurity scattering at temperatures below 250 K.

4.1.2.4 A. Suzuki et al. (1988)

Temperature dependencies of Hall mobilities of undoped and nitrogen-doped n-type ß-SiC films have been analyzed using a conventional theoretical model[34,47]. Considering acoustic, polar optical, and piezoelectric lattice scattering, as well as ionized and neutral impurity scattering, theoretical calculations well fitted to the experimental results are obtained at 70-1000 K.

Single crystals of ß-SiC were epitaxially grown on Si (100) substrates. Prior to CVD growth, a very thin carbonized "buffer" layer (a few tens nm or thiner) was formed on the Si substrate to minimize the effect of lattice mismatch and thermal coefficient differences between SiC and Si. Six kinds of films were used for the measurements, as shown in table 4.2 in appendix 4. Three kinds of undoped films were grown by varying the Si/C ratio in the source gases and the other three kinds of nitrogen-doped films by varying a flow rate of nitogen doping gas.

Experimental data of Hall mobility are shown in figures 4.7a and b in appendix 4. Theoretical method of calculations are carried out as shown in appendix 4. Obtained values of N_D, N_A and N_A/N_D are listed in table 4.4 in appendix 4.

The previous values of N_D and N_A obtained from the analysis of n(T) (table 4.2) for the same films are significantly different from the present results. Both N_D and N_A of the previous analysis are several to ten times larger and the ratios of N_A/N_D are very high for all the films. At the present stage the reason for the differences between two analyses can not be clearly explained. But the theoretical model used for the analysis of n(T) is a simple one considering a single donor level. The films may contain multiple levels. For example, another carrier generation from a deeper level is observed at higher temperatures in the experimental results[32]. If thoselevels are not so deep, they affect the shape of n(T) in the whole

Table 4.2 Donor ionization energies E_D, donor N_D, Acceptor concentrations N_A, and compensation ratio N_A/N_D obtained from a least-squares fit of the data of Suzuki et al. to the single-level expression for the carrier concentration using the band parameters discussed in the source of this table

	Si/C	N_2 flowrate (sccm)	E_D meV	N_D $\times 10^{16}$ cm^{-3}	N_A $\times 10^{16}$ cm^{-3}	N_A/N_D
Nondoped films	0.33	0	20.5	54.2	50.6	0.94
	0.37	0	20.3	37.6	36.2	0.96
	0.40	0	21.7	25.7	25.1	0.96
Nitogen-doped films	0.33	0.05	15.8	216	18	0.83
	0.33	0.15	12.5	336	273	0.81
	0.33	0.45	4.6	764	594	0.78

Source: Segall, B. "comments", Appl. Phys. Lett. 50 (1987): 1534.

temperature range. Moreover, the theoretical fitting for n(T) is not so sensitive to the value of N_A/N_D as shown by Segall et al. [28]. On the other hand, N_A/N_D can be determined much more decisively for the fitting of $\mu_H(T)$, although the theoretical equations contain several assumptions. From these facts, the authors[34] consider that the present analysis of $\mu_H(T)$ better explains all of the experimental results.

4.1.2.5 T. Tachibana et al. (1990)

Hall measurements were conducted at temperatures up to 1000 K on unintentionally doped n-type ß-SiC and α-SiC thin films epitaxially grown on both on-axis and vicinal Si (100) and 6H-SiC thin films epitaxially grown on Si(100) and 6H-

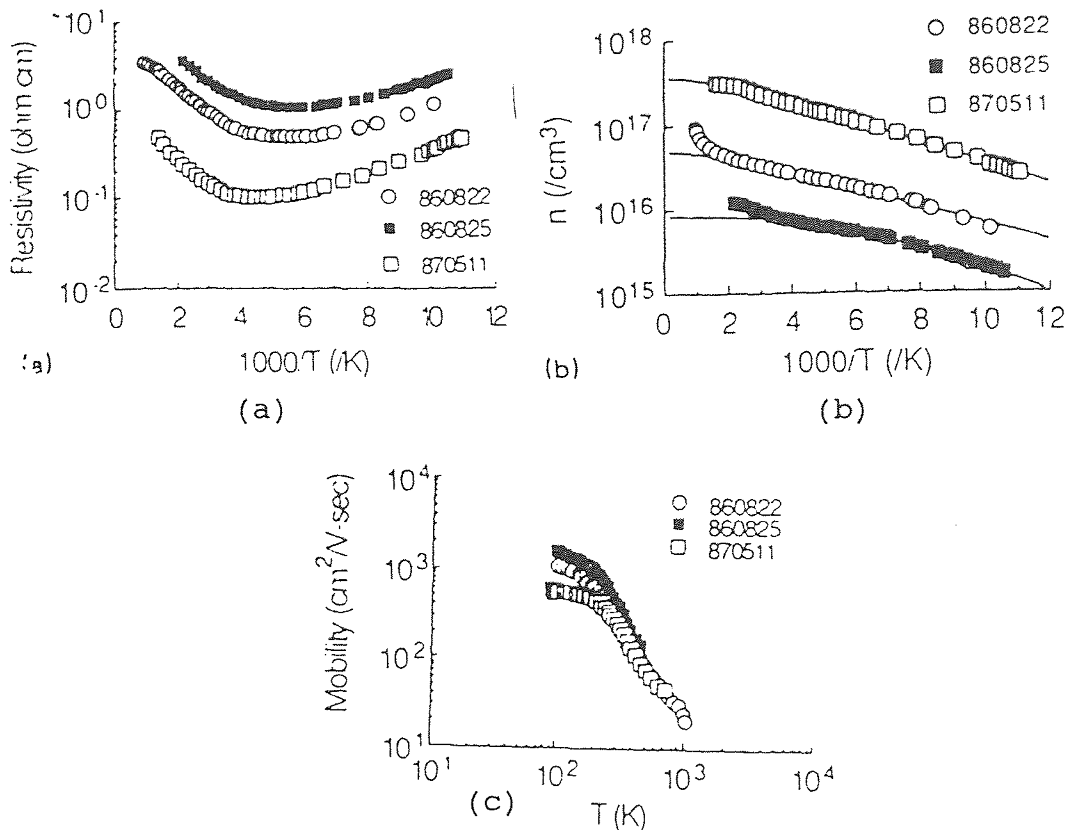

Figure 4.8 Temperature dependence of (a) resistivity, (b) Carrier Concentration (solid lines represent theoretical data), and (c) electron Hall mobility of ß-SiC chemically vapor deposited on Si (100). Numbers shown in the legend refer to experimental sample numbers. See Table 4.5 for data regarding the properties of these films.

SiC(0001) by chemical vapor deposition[24]. The carrier concentration versus temperature data were analyzed using a compensation model (appendix 4).

The results of Hall measurements of resistivity, carrier concentration, and electron mobility on three undoped ß-SiC single-crystal films grown on Si(100) in the temperature range of 87-1000 K are shown in figure 4.8. Film thickness data and those derived from the measurements are given in table 4.5. The three films showed n-type

conduction at all temperatures. The carrier concentration (figure 4.8(b)) increased within the range of 10^{15}-$3X10^{17}$ cm^{-3} while the electron Hall mobility (figure 4.8(c)) decreased on the order of 10^{3}-10^{1} cm^{2}/V s as temperature was increased. The results of the curve-fitting procedures shown as the solid lines in figure 4.8(b) revealed that the films were highly compensated (N_A/N_D > 0.88), and that the values for E_D (14-20meV) were closer to the values reported by Segal (13-17meV) , Yamanaka (18 meV) and Suzuki (20-22meV) than the values reported by **PL** studies (53-54 meV).

Three off-axis ß-SiC samples with (100) oriented 3°-4° toward [011] were similarly measured in the temperature range of 87-1000 K. The results are shown in figure 4.9 in appendix(4). The resistivity, carrier concentration, and electron Hall mobility data showed similar tendencies as the analogous data obtained from the on axis films. Again, all the undoped ß-SiC films showed n-type conduction.

A compensation analysis has also been conducted on the carrier-concentration versus temperature data of the three separately deposited off-axis ß-SiC samples. Equations 4.25 and 4.26 in appendix 4 were applied using the same physical values of M, g, and m^{*}_{e} for on-axis films. The results are shown in table 4.6 appendix 4 and described by the solid lines in figure 2(b). All the crystals were highly compensated (N_A/N_D = 0.73 - 0.94); The doping concentrations were also substantial (10^{17}-10^{18} cm^{-3}). The donor ionization energies were 15-21 meV. It was concluded from this analysis

Table 4.5 Parameters obtained by fitting the compensation model to carrier-concentration vs temperature data obtained for ß-SiC (100) on Si (100)

Samples	Thickness	N_D X10^{18} (cm^{-3})	N_A X10^{18} (cm^{-3})	E_D (meV)	N_A/N_D
860822	18.0	1.23	1.19	16.0	0.97
860825	19.6	4.59	4.50	20.2	0.98
870511	17.7	3.16	2.80	14.4	0.88

Source: T. Tachibana et al. J. Appl. Phys. 67 (1990): 6378.

that there is no difference between on- and off-axis ß-SiC on Si in terms of compensation.

The samples of ß- and α(6H)-SiC grown on α-SiC showed n-type conduction at all temperatures corresponding to those of Hall measurements. The results of these mesurements are shown in figures 4.10 and 4.11 in appendix 4. Compensation analyses have been conducted using the calculated values of carrier concentration versus temperature. Equations 4.25 and 4.26 with the values of M=3, g=2, and m^*_e =0.346m_o (ß) and 0.45 m_o (α) were applied. The results of the analysis are shown in table 4.7 in appendix 4 and as solid lines in figures 4.10(b) and 4.11(b) in appendix 4.

By contrast, undoped ß- and α-SiC films grown on α-SiC substrates were not highly compensated (N_A/N_D=0.36, for ß-SiC on α-SiC, and 0.02, for α-SiC on α-SiC, respectively).

This work indicates that decreasing the defect densities in the films lead to a decrease in the compensation ratio.

CHAPTER 5

CONCLUSION

The work at NCSU demonstrated the feasibility of producing large 6H SiC substrates and also the feasibility of making excellent high temperature SiC devices[1]. It is no longer a question "if" SiC will be successful, but "when".

At this time, the performance of prototype devices that use 6H SiC as a starting material are much superior to those using ß-SiC grown on Si. Hence, The emphasis in CVD growth for device fabrication will probably shift to using 6H-SiC substrates. Much work remains in the development of the seeded-growth sublimation method that will supply these substrates, and in characterizing the resulting material. Research on the method of growing ß-SiC on Si should continue because of the potential economic advantage of starting with inexpensive Si substrates.

ß-SiC and 6H-SiC each have advantages over the other. For example, the simpler structure of ß results in it having a larger electron mobility and an advantage for high fequency devices. The larger band gap of 6H-SiC allows it to be used for blue LEDs, and for operating at higher temperatures than ß-SiC. Hence, There are resons for pursuing both polytypes.

As interest in SiC devices picks up, there must remain a balance between basic materials research and device

research. Some challenges lie ahead in understanding the Source of electrical compensation.

APPENDIX 1

Comparison of Properties of Semiconductors

Table 1.1 Comparison of semiconductors

Property	Si	GaAs	GaP	Beta-SiC (6H-SiC)	Diamond
Bandgap (eV) 300 K	1.1	1.4	2.3	2.2 (2.9)	5.5
Melting Point (C)	1420	1238	1470	Sublimes > 1800	phase change
Max. Operating Temperature (C)	300	460	925	873	1100 (1240)
Physical stability	Good	Fair	Fair	Excellent	very good
Electron mobility R.T. $cm^2/V\text{-}s$	1400	8500	350	*1000	2200
Hole mobility R.T., $cm^2/V\text{-}s$	600	400	100	40	1600
Breakdown voltage $X10^6$ V/cm	0.3	0.4	-	4.0	10.0
Thermal conductivity, W/cm-C	1.5	0.5	0.8	5.0	20.0
Sat. elec. drift vel. 10^7 cm/s	1.0	2.0	-	2.5	2.7
Dielectric const. k	11.8	12.8	11.1	9.7	5.5

* Room temperature electron mobility has been reported to be in the range of 245 to 310 $cm^2/V.s$ by B. Segall [28].

APPENDIX 2

The More Common SiC Polytypes

Table 2.2 Selected SiC Polytypes

	Ramsdel notation	Stacking sequence
(Cubic or ß)	3C	ABC/ABC....
α	6H	ABCACB/ABCACB/....
	15R	ABCBACABACBCACB/AB...
	4H	ABAC/ABAC...
	2H	AB/AB... .

Source: Powell J.A. and L.G. Matus. "Recent Developments in SiC (USA)." Proceedings of the First International conferance., Washington DC (1987): 2-3.

The more common SiC polytypes are listed in table 2.2. Several ways of designating the various structures are shown in this table. The most common is the Ramsdel notation which is a number followed by a letter. The number is the number of the double layers in a stacking repeat sequence and the letter designates the structure. Thus, we have 3C for cubic SiC. All of the other polytypes are known as α-SiC . The most common is 6H-SiC. There realy are only two polytypes of practical importance, ß-SiC (the only cubic form) and 6H-SiC.

Appendix 3

SiC Phase Diagram and Growth Rates vs Temperature, Pressure and Flowrate

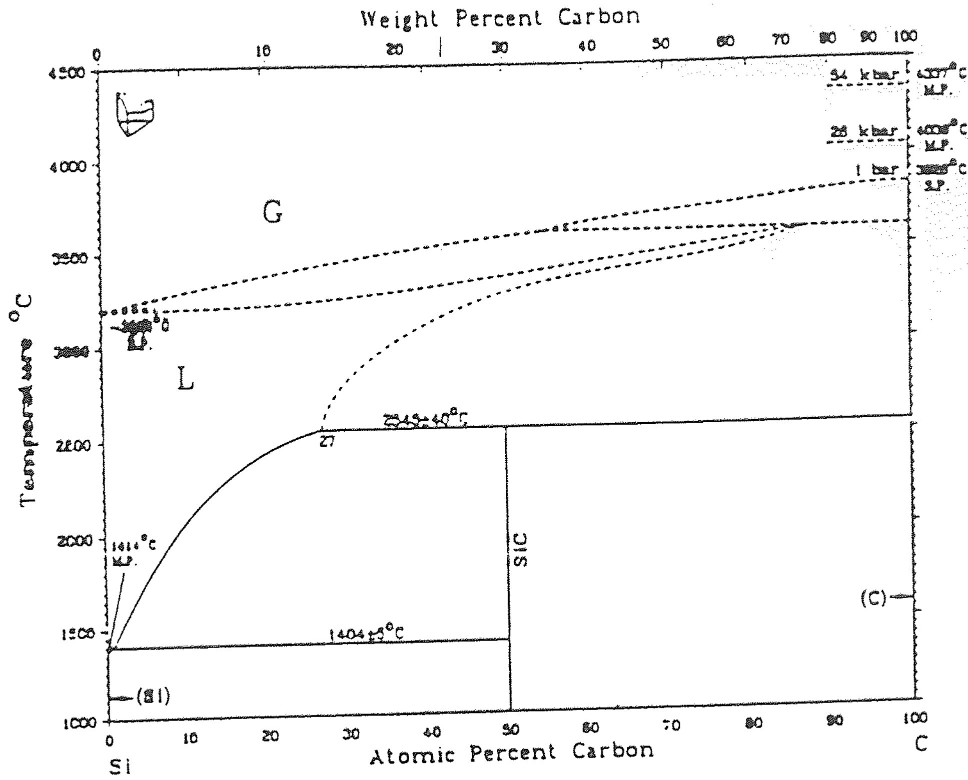

Figure 3.4 Phase Diagram of SiC

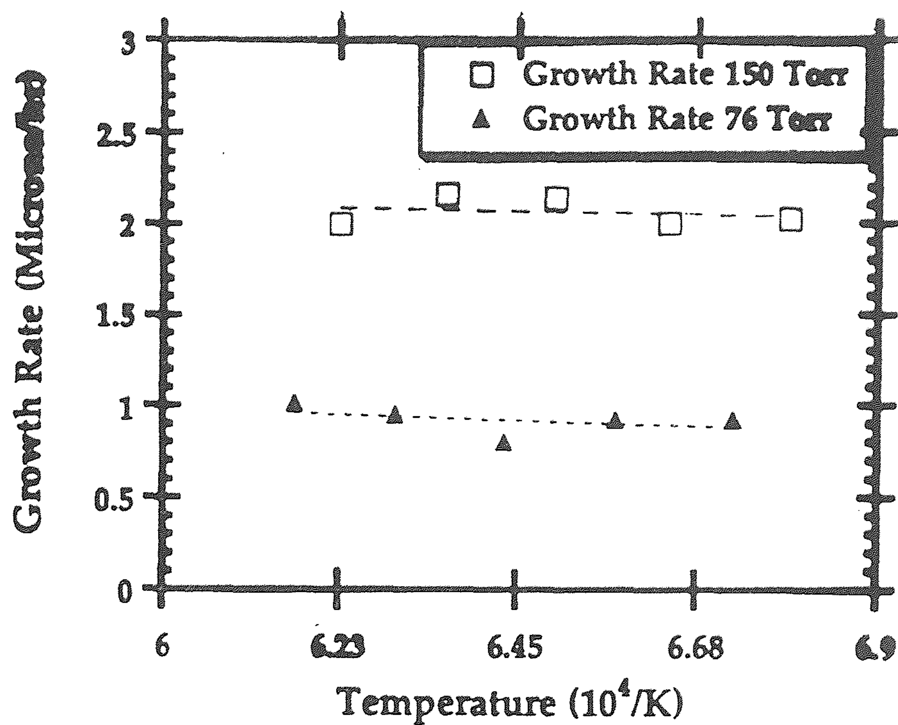

(a)

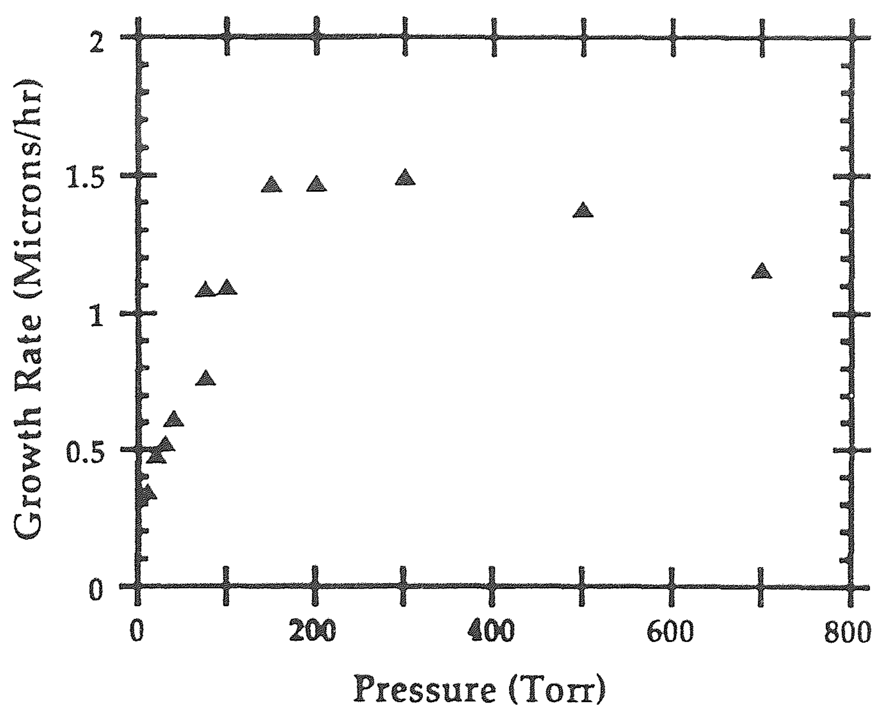

(b)

Figure 3.5 (a) Growth Rate (μm/hr) vs. Temperature (10^4/°K)
(b) Growth Rate (μm/hr) vs. Pressure (Torr)

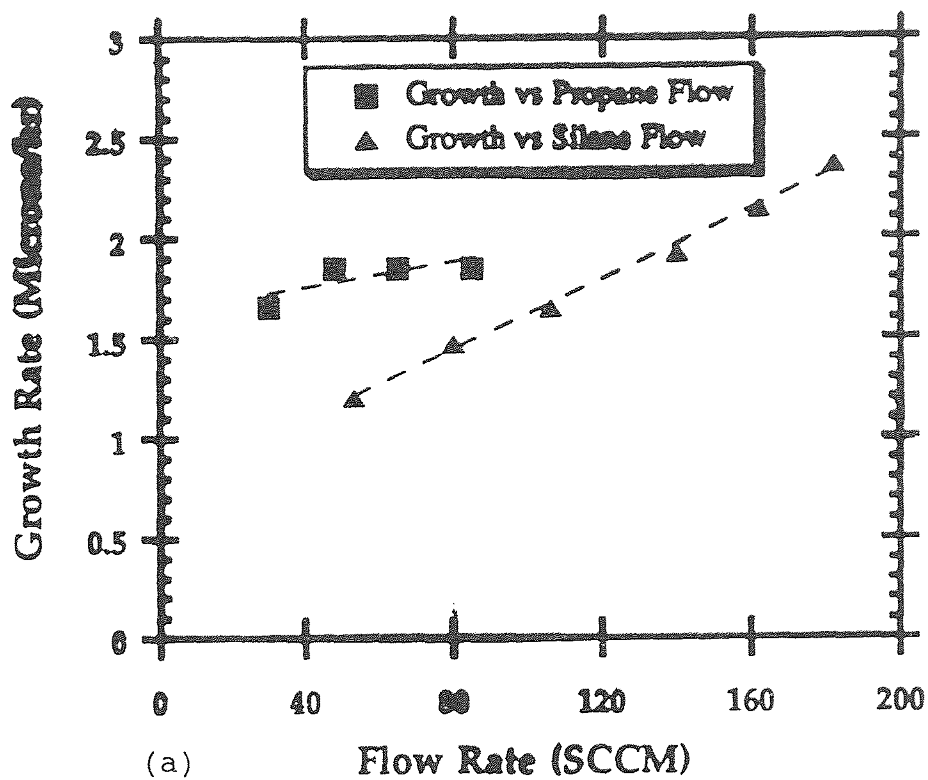

(a)

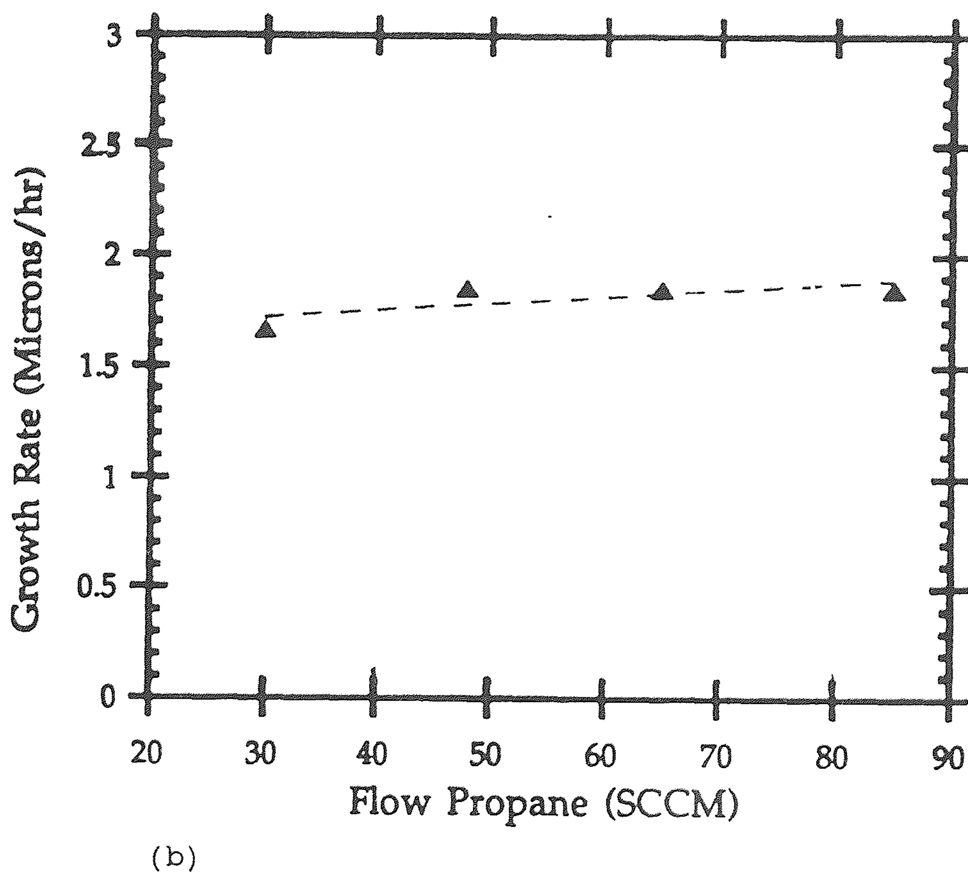

(b)

Figure 3.6 (a,b) Growth Rate (μm/hr) vs. Flow rate (SCCM)

APPENDIX 4

Theoretical Calculation of Hall Mobility and Compensation Model

Three modes of lattice scattering due to acoustic phonon, polar optical phonon, and piezoelectric scattering, and two modes of impurity scattering due to ionized impurity and neutral impurity are considered.

Conductivity mobility μ_i for each lattice scattering i at temperature T is expressed as follows.

For acoustic-mode lattice scattering,

$$\mu_{ac}=C_{ac}E_{ac}^{-2}(m/m_\circ)^{-5/2}T^{-3/2} \quad (4.3)$$

$$C_{ac}=2/3(2\pi)^{1/2}q(h/2\pi)^4 m_\circ^{-5/2}U_l^2 D \quad (4.4)$$

where E_{ac} is the deformation potential, m the effective mass, U_l the sound velocity of longitudinal mode, D the density, $m_\circ$ the free electron mass, q the elementry charge, h the Planck constant, and k the Boltzmann constant. The Hall factor β_{ac} is $3\pi/8$.

For Polar optical-mode lattice scattering,

$$\mu_{pol}=C_{pol}(m/m_\circ)=^{-3/2}z^{-1/2}\ x(z)[\exp(z)-1] \quad (4.5)$$

$$C_{pol}=(32/3)2^{-1/2}\pi^{1/2}q^{-1}(h/2\pi)^{3/2}m_\circ^{-3/2}$$
$$w_l^{-1/2}\ (\epsilon_{opt}^{-1}-\epsilon^{-1})^{-1} \quad (4.6)$$

$$z=\theta/T \quad (4.7)$$

where w_l is the frequency for longitudinal optical mode, ϵ_{opt} and ϵ are the optical and the static permittivities,

respectively, and θ is the characteristic temperature. The function $x(z)$ varies from 0.6 to 2.8 in the present calculation[50]. The Hall factor β_{pol} varies from 1.00 to 1.14 depending on z[51].

For piezoelectric-mode lattice scattering,

$$\mu_{piez}=C_{piez}(m/m_{\circ})^{-3/2}T^{-1/2} \qquad (4.8)$$

$$C_{piez}=(16/3)(2\pi)^{1/2}(h/2\pi)^{2}q^{-1}m_{\circ}^{-3/2} \quad k^{-1/2}\alpha^{-1}(\epsilon/K_{14}{}^{2}) \qquad (4.9)$$

$$K_{14}{}^{2}=e_{14}{}^{2}(\epsilon C_{11})^{-1} \qquad (4.10)$$

$$\alpha=(16/13)(1+2C_{12}/C_{11}+4C_{44}/C_{11} +4K_{14}{}^{2})^{-1}+(6/13)(C_{44}/C_{11}+K_{14}{}^{2})^{-1} \qquad (4.11)$$

where e_{14} is the piezoelectric constant, and C_{11}, C_{12}, and C_{44} are the elastic constants. The Hall factor β_{piez} is 1.10.

For simplicity, Hall mobility $\mu_i{}^H$, due to each scattering mode i, is assumed to be expressed as a product of the corresponding Hall factor β_i and conductivity mobility μ_i.
Moreover, combined Hall mobility $\mu^{H}{}_{lattice}$ is expressed as follows:

$$(\mu^{H}{}_{lattice})^{-1}=(\mu_{ac}{}^{H})^{-1}+(\mu_{pol}{}^{H})^{-1} +(\mu_{piez}{}^{H})^{-1} \qquad (4.12)$$

The theoretical values for the constants of ß-SiC are shown in table 4.3 in appendix 4.

Conductivity mobilities for impurity scattering are calculated as follows[47].

For ionized-impurity scattering,

$$\mu_{ion}=C_{ion}(m/m_\circ)^{-1/2}N_i^{-1}T^{3/2}[f(b)]^{-1} \quad (4.13)$$

$$C_{ion}=128X2^{1/2}\pi^{1/2}k^{3/2}\epsilon^2q^{-3}m_\circ^{-1/2} \quad (4.14)$$

$$f(b)=\ln(1+b)-b/(1+b) \quad (4.15)$$

$$b=C'_{ion}\ N'_i{}^{-1}(m/m_\circ)T^2 \quad (4.16)$$

$$C'_{ion}=24\epsilon k^2(h/2\pi)^{-2}m_\circ q^{-2} \quad (4.17)$$

$$N_i=n+2N_A \quad (4.18)$$

$$N'_i=n+(n+N_A)[1-(n+N_A)/N_D] \quad (4.19)$$

where n is the electron concentration at temperature T, N_i the ionized-impurity concentration. The Hall factor $ß_{ion}$ varies from 1.2 to 1.9 depending on b[47].

For neutral-impurity scattering,

$$\mu_{neu}=C_{neu}N_n^{-1}(m/m_\circ) \quad (4.20)$$

$$C_{neu}=(80\pi)^{-1}m_\circ q^3\epsilon^{-1}(h/2\pi)^{-3} \quad (4.21)$$

$$N_n=N_D-N_A-n \quad (2.22)$$

where N_n is the neutral-impurity concentration. The Hall factor $ß_{neu}$ is unity.

Combined Hall mobility $\mu^H{}_{imp}$ and the total Hall mobility $\mu^H{}_{tot}$ for lattice and impurity scattering are assumed to be expressed as follows:

$$(\mu^H{}_{imp})^{-1}=(\mu^H{}_{ion})^{-1}+(\mu^H{}_{neu})^{-1} \tag{4.23}$$

$$(\mu^H{}_{tot})^{-1}=(\mu^H{}_{lattice})^{-1}+(\mu^H{}_{imp})^{-1} \tag{4.24}$$

Table 4.3 Numerical values used for theoretical calculations.

Constants	Values
E_{ac}	22 eV
U_l	1.0×10^{4} m/s
D	3.2×10^{3} kg/m^{3}
w_l	1.83×10^{14} s^{-1}
ϵ_{opt}	5.77×10^{-11} F/m
ϵ	8.61×10^{-11} F/m
Θ	1399 K
e_{14}	0.17 c/m^{2}
C_{11}	2.89×10^{11} N/m
C_{12}	2.34×10^{11} N/m
C_{44}	5.54×10^{10} N/m

Source: Daal, H.J. van Mobility of charge carriers in Silicon Carbide (Philips Res. Rep. Suppl. 3 (1965): 48, as cited in Suzuki, A. et al. J. Appl. Phys. 64 (1988): 2820

Table 4.4 Donor concentration N_D, Acceptor concentration N_A, and compensation ratio N_A/N_D obtained from theoretical calculations fitted to the experimental data of Hall mobility

	Si/C	N_2 flowrate (sccm)	N_D $\times 10^{16}$ cm^{-3}	N_A $\times 10^{16}$ cm^{-3}	N_A/N_D
Nondoped films	0.33	0	6.6	3.0	0.45
	0.37	0	5.6	4.2	0.75
	0.40	0	15.0	14.4	0.96
Nitogen-doped films	0.33	0.05	48	12	0.25
	0.33	0.15	90	27	0.30
	0.33	0.45	230	57	0.25

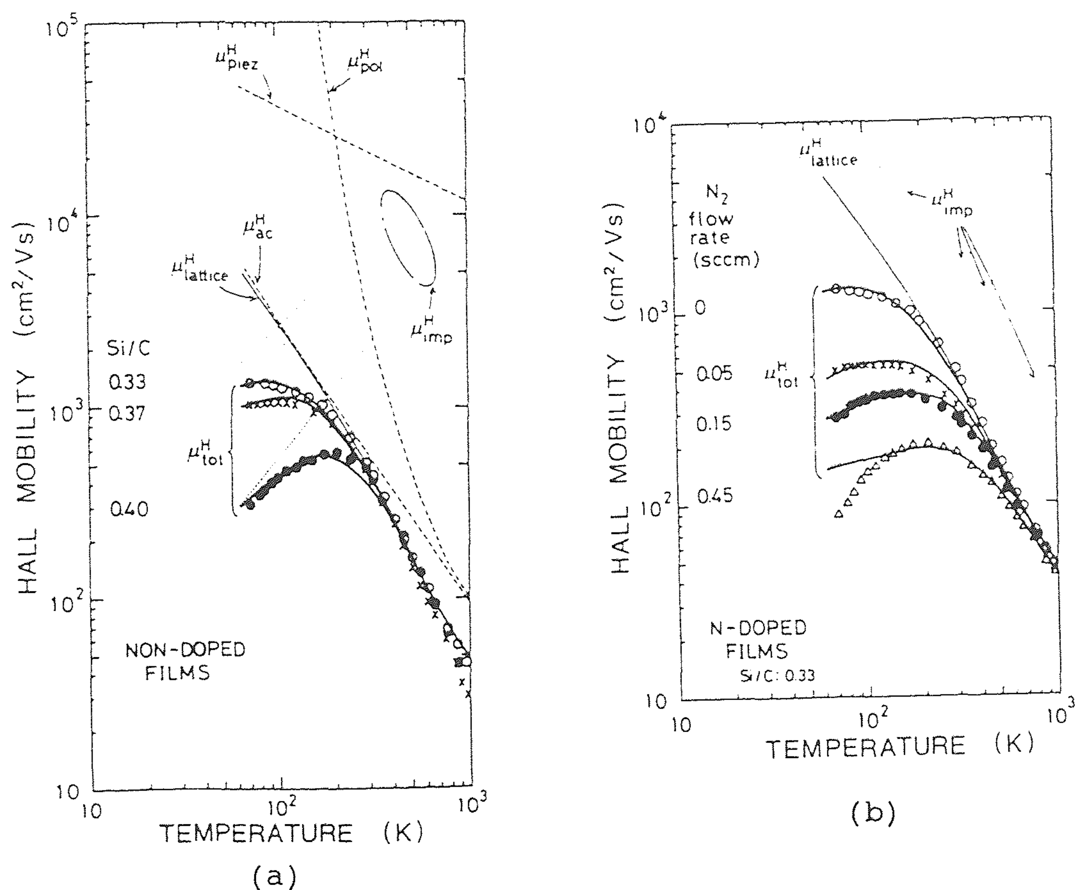

Figure 4.7 Temperature dependencies of Hall mobility of (a) undoped. (b) Nitrogen-doped films. Solid, broken, and dotted lines are calculated values.

Compensation Model

For a nondegenerate, n-type semiconductor with a shallow donor; the working equation is

$$n_o(n_o+N_A) = (N_D-N_A-n_o)\ (N_C/g)\ \exp(-E_D/kT) \qquad (4.25)$$

where n_o is the free-electron density in the conduction band, g is the degeneracy factor, and k is the Boltzman constant. N_C is the density of states and is given by

$$N_C = (2M)\ (2\pi m_e^{*}\ kT/h^2)^{1.5} \qquad (4.26)$$

in which M is the number of equivalent minima in the conduction band and m_e^{*} is the density-of-states effective mass of electrons.

It has been shown in luminescence syudies that the conduction-band minima lie along the <100> axis on the Delta band, which produces a spin-degeneracy factor g = 2.

Since ß-SiC has the zinc-blende structure, it is quite reasonable to expect each minima to be at a zone boundry and thus M = 3 [52].

The value of m_e^{*} is given by $(m_t^2 m_l)^{0.33}$, where m_t and m_l are the transverse and longitudinal masses, respectively. The values of $m_t = 0.346m_o$ is obtained from the values of $m_t = 0.247m_o$ and $m_l = 0.677m_o$, as determined by cyclotron resonance measurements [53].

The values of N_D, N_A, and E_D are adjusted so that the resulting theoretical curves have the least deviation from the data points in plots of the experimental curves of carrier concentration versus temperature.

Table 4.6 Parameters obtained by fitting the compensation model of carrier-concentration vs temperature data obtained for ß-SiC (100) on off-axis Si (100).

Samples	Thicknes	N_D X10^{18} (cm^{-3})	N_A X10^{18} (cm^{-3})	E_D (meV)	N_A/N_D
870626	5.05	1.37	1.29	16.3	0.94
880329	5.09	1.19	0.86	20.05	0.73
880519	7.32	4.42	3.82	14.7	0.86

Source: T. Tachibana et al. J. Appl. Phys. 67 (1990): 6378.

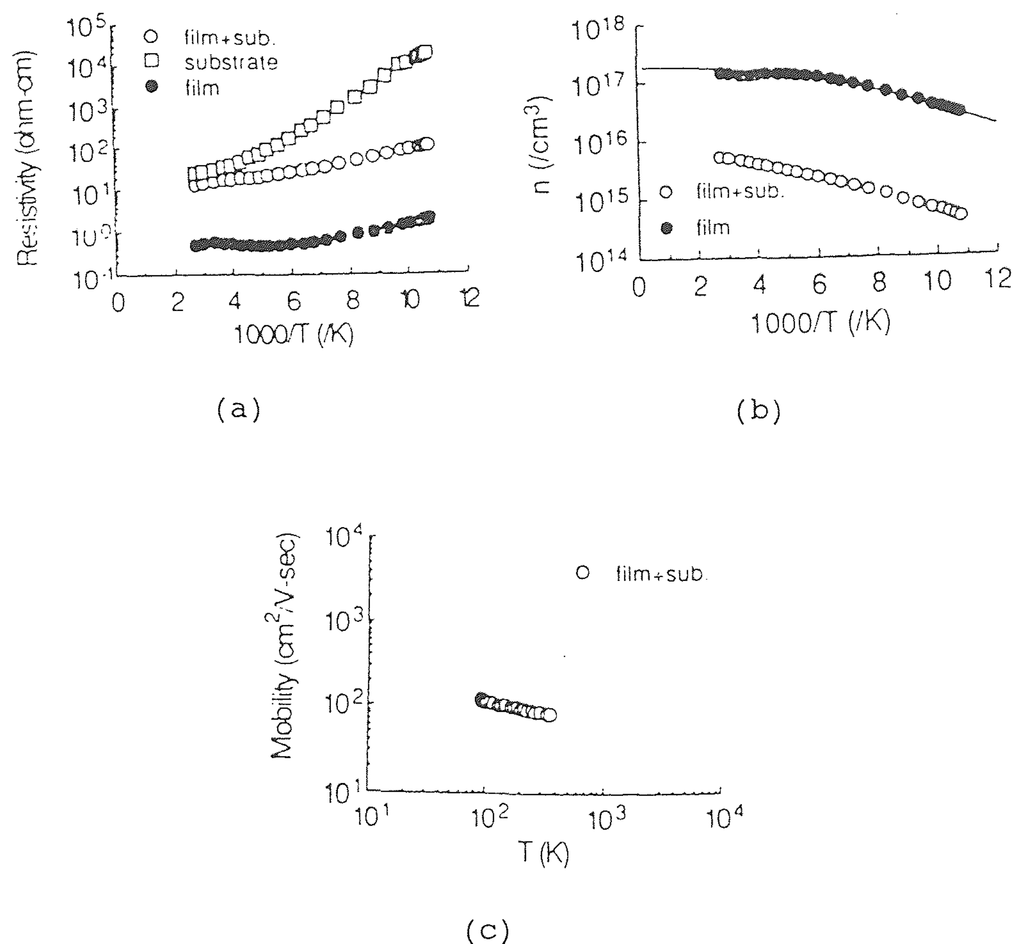

Figure 4.9 Temperature dependence of (a) resistivity, (b) carrier concentration (solid line represents theoretical calculations), and (c) electron Hall mobility of ß-SiC chemically vapor deposited on off-axis Si (100). Numbers shown in the legend refer to experimental sample numbers. See table 4.6 for data regarding the properties of these films.

Table 4.7 Parameters obtained by fitting the compensation model to the values of carrier-concentration vs temperature calculated by assuming the resistivity of the substrate for carrier concentration vs temperature for unintentionally doped ß-SiC and α-SiC grown directly on Lely crystals.

Samples	Thicknes	N_D X10^{18} (cm^{-3})	N_A X10^{18} (cm^{-3})	E_D (meV)	N_A/N_D
ß on α	5.0	0.31	0.11	16.0	0.36
α on α	5.0	789.0	14.6	20.2	0.02

Source: T. Tachibana et al. J. Appl. Phys. 67 (1990): 6378.

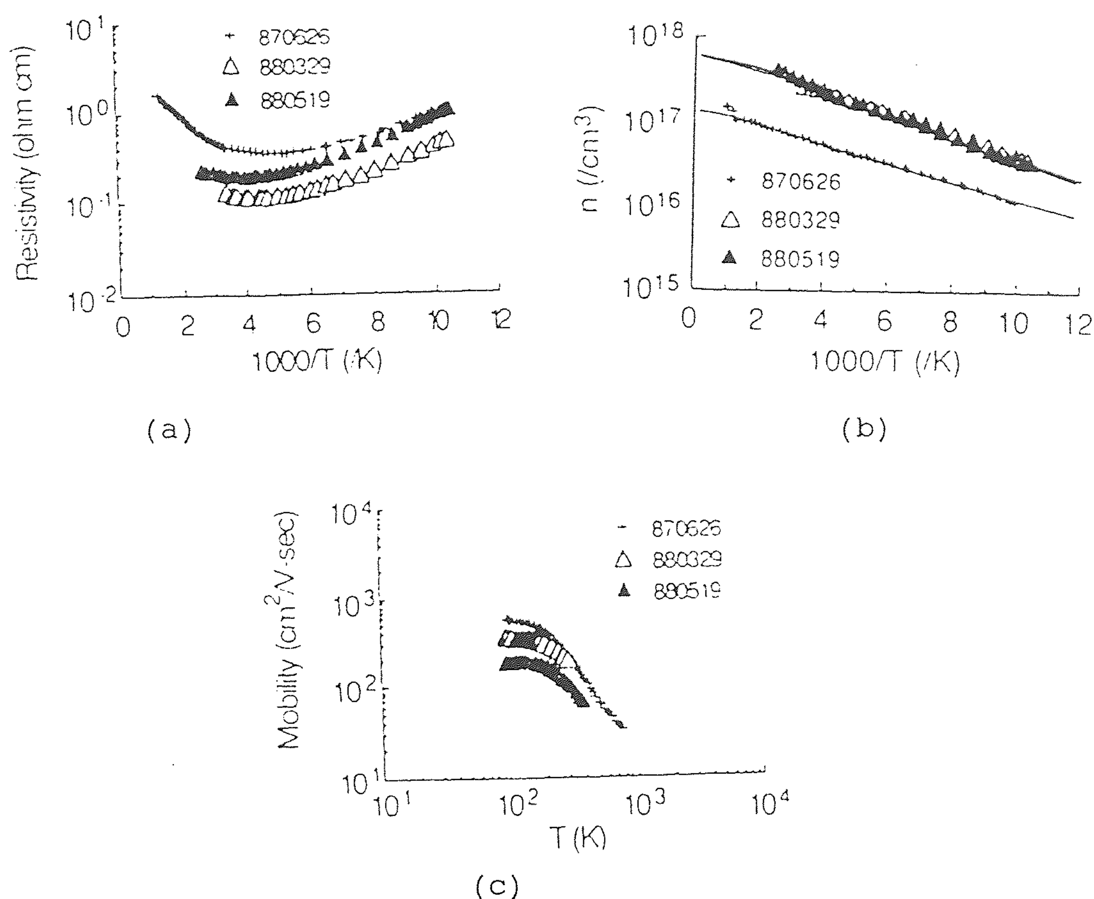

Figure 4.10 Temperature dependence of (a) resistivity, (b) carrier concentration (solid line represents theoretical calculations), and (c) electron Hall mobility of an undoped ß-SiC (111) film grown directly on an α(6H)-SiC (0001) Lely crystal. In (a) the estimated values (substrate) and the calculated values for the grown film (film) are also plotted. In (b) the values for the grown film calculated (film) using the estimated values of resistivity are also plotted. See table 4.7 for data regarding the properties of this sample.

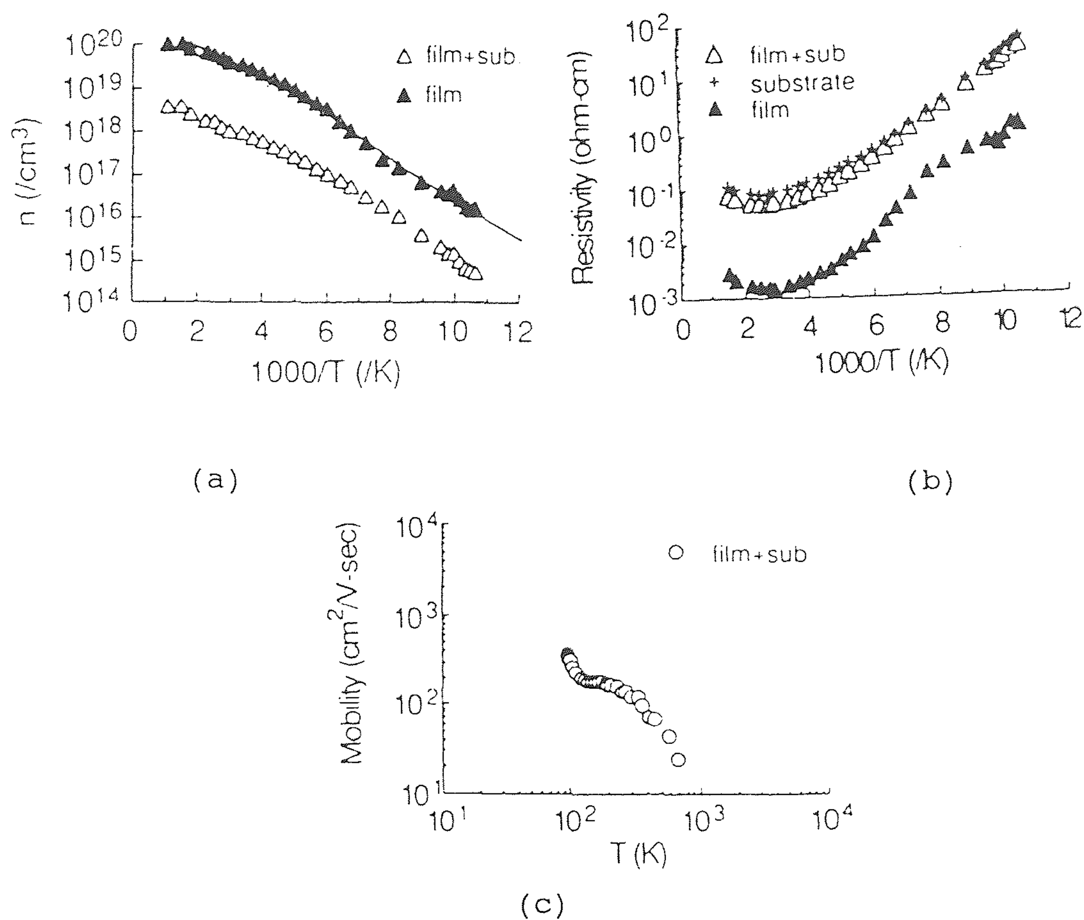

Figure 4.11 Temperature dependence of (a) resistivity, (b) carrier concentration (solid line represents theoretical calculations), and (c) electron Hall mobility of an undoped α-SiC film grown directly on an off-axis α(6H)-SiC Lely crystal. In (a) the estimated values (substrate) and the calculated values for the grown film (film) are also plotted. In (b) the values for the grown film calculated (film) using the estimated values of resistivity are also plotted. See table 4.7 for data regarding the properties of this sample.

REFERENCES

1. Powell, J.A. and L.G. Matus. "Recent Developments in SiC (USA)." *Proceedings of the First International Conference*. Washington DC (1987): 2.

2. Verma, A.R. and P. Krishna *Polymorphism and Polytypism in Crystals*. New York: John Wiley & Sons (1966).

3. Davis, R.E. and K.D. Gailey and K.W. Whitten. "Covalent Bonding II: Valence Bond Theory and Molecular Orbital Theory." *Principles of Chemistry*. Philadelphia: Saunders college (1984): 249.

4. Parthe, E. *Crystal Chemistry of Tetrahedral Structures*. New York: Gordon and Breach (1964).

5. Acheson, E.G. "On Carborundum." *Chemi. News* 68 (1893): 179, as cited in Verma, A.R. and P. Krishna Polymorphism and Polytypism in crystals. New York: John Wiley & Sons (1966).

6. Acheson, E.G. "Carborundum: its history, manufacture and uses." *J. Franklin Inst*. 136 (1893): 194-203, 279-287. as cited in Verma, A.R. and P. Krishna *Polymorphism and Polytypism in Crystals*. New York: John Wiley & Sons (1966).

7. Lely, J.A. Ber. Dt. Kerma. Ges. 32 (1955): 229, as cited in Powell, J.A. and L.G. Matus. "Recent Developments in SiC (USA)." *Poceedings of the First International Conference. Washington DC* (1987): 5.

8. Nelson, W.E. et al. *J. Appl. Phys*. 37 (1966): 333. as cited in Powell, J.A. and L.G. Matus. "Recent Developments in SiC (USA)." *Proceedings of the First International Conference*. Washington DC (1987): 5.

9. Knippenberg, W.F. and G. Verspui *Philips Res. Repts*. 21 (1966): 113, as cited in Powel, J.A. and L.G. Matus.

10. Nishino, S. et al. *Appl. Phys. Lett*. 42 (1983): 460, as cited in Powel, J.A. and L.G. Matus.

11. Carter,Jr. C.H. et al. presented at the *Fourth National Review Meeting on the Growth and Characterization of SiC*, Raleigh, NC (1987), as cited in Powel, J.A. and L.G. Matus.

12. Moers, K. "Methods for the preparation of pure high-melting carbides, nitrides and borides and a description of a few of their properties." *Z. Anorg. Allgem. Chem.* 198 (1931): 233-243, 243-261, 262-275, as cited in Verma, A.R. and P. Krishna.

13. Lely, J.A. "Darstellung von Einkristallen von Silicium-carbide und Behrrschung von Art und Menge der eingebauter verunreinigungen. Ber. Deut. Keram. Ges". 32 (1955):229-231, as cited in Verma, A.R. and P. Krishna.

14. Knippenberg, W.F." Growth phenomena in silicon carbide." *Philipis Res. Rept.* 18 (1963): 161-274, as cited in Verma, A.R. and P.Krishna.

15. Glasow, P.A. "Recent Developments in SiC (USA)." *Proceedings of the First International Conferrence.* Washington DC (1987): 16

16. Tairov, Y.M. and V.F. Tsvetkov *J. Cryst. Growth* 43 (1978): 209, as cited in Powell, J.A. and L.G. Matus.

17. Tairov, Y.M. and V.F. Tsvetkov *J. Cryst. Growth* 52 (1981): 146, as cited in Powell, J.A. and L.G. MAtus.

18. Ziegler, G. et al. *I.E.E.E. Trans. Electron Devices ED-30* (1983): 277, as cited in Powell, J.A. and L.G. Matus.

19. Powell, J.A. *Proc. Mats. Res. Soc. Symp.* 97 (1987): 159. as cited in Powell, J.A. and L.G. Matus.

20. Powell, J.A. et al. *J. Electrochem. Soc.* 134 (1987): 1558, as cited in Powell, J.A. and L.G. Matus.

21. Bonfield. T.D. "Plasma Assisted Chemical Vapor Deposition." *Deposition Technologies for Films and Coatings*. Park Ridge NJ: Noyes Publications, p365.

22. Knight, J.C. *Symposia Proceedings of Material Science Research Society Fall 1984 Meeting* 38 (1985): 371-381, as cited in Nguyen, V.S. "Plasma Assisted Chemical Vapor Deposition." *Hand Book of Thin-Film Deposition Processes and Techniques*. Park Ridge NJ: Noyes Publications, p120.

23. Dun, H. et al. *J. Electrochem. Soc.* 128 (1981): 1556, as cited in Nguyen, V.S. "Plasma Assisted Chemical Vapor Deposition." *Hand Book of Thin-Film Deposition Processes and Techniques*. Park Ridge NJ: Nyes Publications, p120

24. Tachibana, T. et al. "Hall Measurements as a Function of Temperature on Monocrystalline SiC Thin Films." *J. Appl. Phys.* 67 (1990): 6375.

25. Sasuki, K. et al. *Appl. Phys. Lett.* 45 (1984): 72.

26. Dean, J.P. et al. 15 (1977): 299.

27. Choyke, W.J. and L. Patrick "Silicon Carbide 1973" edited by R.C. Marshal, J.W. Faust and C.E. Ryan (University of South Carolina Columbia, SC, 1974), p. 261.

28. Segall, B. et al. *Appl. Phys. Lett.* 49 (1986): 584.

29. Segall, B. et al. *Appl. Phys. Lett.* 50 (1987): 1533.

30. Aivazova, L.S. et al. *Sov. Phys. Semicond.* 11 (1977): 1069.

31. Yamanaka, M. et al. *J. Appl. Phys.* 61 (1987): 599.

32. Suzuki, A. et al. *Appl. Phys. Lett.* 49 (1986): 450.

33. Suzuki, A. et al. *Appl. Phys. Lett.* 50 (1987): 1534.

34. Suzuki, A. et al. *Appl. Phys. Lett.* 64 (1988): 2818.

35. Dall, H.J. van *Philips. Res. Rep. Suppl.* 20 (1965): 1.

36. Carlos, W.E. et al."Novel Refractory Semiconductors." *Materials Research Society Proceedings,* Vol. 97 edited by D.Emin, T.L. Aselage and C. Wood (material Research society, Pittsburg, PA, 1987), p. 253.

37. Freitas, A. et al. *Appl. Phys. Lett.* 52 (1988): 1695.

38. Wang, C. et al. *Phys. Rev.* B 38 (1988): 12752.

39. Birnie, D.P. *J. Am. Ceram. Soc.* 69 C-33 (1986).

40. Dall, H.J. van *Philips Res. Rept. Suppl.* 3 (1965): 25-70.

41. Pauw, L.J. van der *Philips Res. Rept.* 13 (1958): 1.

42. Barrett, D.L. and R.B. Campbell *J. Appl. Phys.* 38 (1967): 53.

43. Kang, H. R.B. Hilborn "Silicon Carbide-1973", edited by R.C. Marshall, J.W. Faust and C.E. Ryan (University of South Carolina, Columbia, South Carolina, 1974), p. 493.

44. Patrick, L. *J. Appl. Phys.* 38 (1967): 50.

45. Patrick, L.J. *J. Appl. Phys.* 37 (1966): 4911.

46. Bevington, P.R. *Data Reduction and Error Analysis for the Physical Sciences.* New York: Mc Graw Hill (1969): Chapter 11

47. Dall, H.J. van "Mobility of Charge Carriers in Silicon Carbide." *Philips Res. Rept.* Suppl. 3 (1965): 48.

48. Pearson, G.L. and J. Bardeen *Phys. Rev.* 75 (1949): 865.

49. Debye, P.P. and E.M. Conwell *Phys. Rev.* 93 (1954): 693.

50. Howarth, D.J. and E.H. Sondheimer *Proc. R. Soc.* London Ser. A 219 (1953): 53.

51. Lewis, B.F. and E.H. Sondheimer *Proc. R. Soc.* London Ser. A 227 (1954): 241.

52. Choyke, W.J. et al. *Phys. Rev.* 133, A1163 (1964).

53. Kaplan, R. et al. *Solid State Commun.* 55 (1985): 67.